Redox Biology 67 (2023) 102937

Contents lists available at ScienceDirect

Redox Biology

journal homepage: www.elsevier.com/locate/redox

Cardiomyocyte NOX4 regulates resident macrophage-mediated inflammation and diastolic dysfunction in stress cardiomyopathy

Aleksandr E. Vendrov [a], Han Xiao [b,c,d,e,f], Andrey Lozhkin [a], Takayuki Hayami [a], Guomin Hu [b,c,d,e,f], Matthew J. Brody [g,h], Junichi Sadoshima [i], You-Yi Zhang [b,c,d,e,f], Marschall S. Runge [a], Nageswara R. Madamanchi [a,*]

[a] Frankel Cardiovascular Center, Division of Cardiovascular Medicine, Department of Internal Medicine, University of Michigan, Ann Arbor, MI, 48109, USA
[b] Department of Cardiology and Institute of Vascular Medicine, Peking University Third Hospital, Beijing, 100191, China
[c] NHC Key Laboratory of Cardiovascular Molecular Biology and Regulatory Peptides, Beijing, 100191, China
[d] Key Laboratory of Molecular Cardiovascular Science, Ministry of Education, Beijing, 100191, China
[e] Beijing Key Laboratory of Cardiovascular Receptors Research, Beijing, 100191, China
[f] Research Unit of Medical Science Research Management/Basic and Clinical Research of Metabolic Cardiovascular Diseases, Chinese Academy of Medical Sciences, Beijing, 100191, China
[g] Department of Pharmacology, University of Michigan, Ann Arbor, MI, 48109, USA
[h] Department of Internal Medicine, University of Michigan, Ann Arbor, MI, 48109, USA
[i] Rutgers New Jersey Medical School, Department of Cell Biology and Molecular Medicine, Rutgers Biomedical and Health Sciences, Newark, NJ, 07101, USA

ARTICLE INFO

Keywords:
Cardiomyopathy
Cardiomyocyte mitochondria
Resident macrophages
Cardiac fibroblasts
NADPH oxidase 4
Diastolic dysfunction

ABSTRACT

In acute sympathetic stress, catecholamine overload can lead to stress cardiomyopathy. We tested the hypothesis that cardiomyocyte NOX4 (NADPH oxidase 4)-dependent mitochondrial oxidative stress mediates inflammation and diastolic dysfunction in stress cardiomyopathy. Isoproterenol (ISO; 5 mg/kg) injection induced sympathetic stress in wild-type and cardiomyocyte (CM)-specific *Nox4* knockout (*Nox4*$^{CM-/-}$) mice. Wild-type mice treated with ISO showed higher CM NOX4 expression, H_2O_2 levels, inflammasome activation, and IL18, IL6, CCL2, and TNFα levels than *Nox4*$^{CM-/-}$ mice. Spectral flow cytometry and t-SNE analysis of cardiac cell suspensions showed significant increases in pro-inflammatory and pro-fibrotic embryonic-derived resident (CCR2^{-}MHCII^{hi}CX3CR1^{hi}) macrophages in wild-type mice 3 days after ISO treatment, whereas *Nox4*$^{CM-/-}$ mice had a higher proportion of embryonic-derived resident tissue-repair (CCR2^{-}MHCII^{lo}CX3CR1^{lo}) macrophages. A significant increase in cardiac fibroblast activation and interstitial collagen deposition and a restrictive pattern of diastolic dysfunction with increased filling pressure was observed in wild-type hearts compared with *Nox4*$^{CM-/-}$ 7 days post-ISO. A selective NOX4 inhibitor, GKT137831, reduced myocardial mitochondrial ROS, macrophage infiltration, and fibrosis in ISO-injected wild-type mice, and preserved diastolic function. Our data suggest sympathetic overstimulation induces resident macrophage (CCR2^{-}MHCII^{+}) activation and myocardial inflammation, resulting in fibrosis and impaired diastolic function mediated by CM NOX4-dependent ROS.

1. Introduction

A catecholamine overload induced by stress in adulthood can lead to cardiotoxic effects mediated by hyperactivation of β-adrenergic receptors. Stress cardiomyopathy is an acute heart failure syndrome characterized by transient ventricular dysfunction with various ventricular wall abnormalities caused by sympathetic overstimulation [1]. Although the pathophysiology of stress cardiomyopathy is not fully understood, it is suggested that significant emotional or physical stress precedes the onset of symptomatic cardiomyopathy [2]. With clinical presentation similar to acute coronary syndrome (ACS), stress cardiomyopathy is identified in 1–2% of suspected ACS cases [3]. The clinical

Abbreviations: CM, cardiomyocyte; ISO, isoproterenol; LV, left ventricle; NOX, NADPH oxidase; ROS, reactive oxygen species; t-SNE, t-distributed stochastic neighbor embedding.

* Corresponding author. Department of Internal Medicine, University of Michigan, 7301A Medical Science Research Building III, 1150 W. Medical Center Dr., Ann Arbor, MI, 48109-5644, USA.
E-mail address: madamanc@med.umich.edu (N.R. Madamanchi).

https://doi.org/10.1016/j.redox.2023.102937
Received 31 August 2023; Received in revised form 6 October 2023; Accepted 17 October 2023
Available online 19 October 2023

course of stress cardiomyopathy is commonly characterized by favorable short-term outcomes with complete recovery of left ventricle (LV) function.

In the early stages, stress cardiomyopathy patients have increased LV stiffness and end-diastolic pressure associated with an upward shift in the diastolic pressure-volume relation [4]. Recent studies suggest that stress cardiomyopathy may present with slowly recovering myocardial inflammation [5,6]. Moreover, some degree of diastolic dysfunction may persist in many patients despite recovered global LV ejection fraction and chamber size [7]. Similarly, a study of stable patients with pheochromocytoma without known cardiovascular disease showed that subclinical cardiac dysfunction and fibrosis persisted even after curative surgical treatment [8]. Eventually, these patients may progress to a persistent heart failure phenotype. The precise mechanisms regulating these long-term changes are not known. Hence, the preservation of cardiac function requires an understanding of the molecular mechanisms underlying stress cardiomyopathy and the development of novel therapeutic strategies.

Excessive systemic sympathetic stimulation has direct effects on cardiomyocyte (CM) function, causing myocardial inflammation and damage [9]. Overstimulation of cardiac β-adrenoreceptor in mice activates NACHT, LRR, and PYD domains-containing protein 3 (NLRP3) inflammasome, leading to increased release of the inflammatory cytokine IL18, but not IL1β [10]. This, in turn, results in galectin-3-mediated cardiac inflammation with macrophage infiltration and subsequent pathological cardiac remodeling and dysfunction [11]. Furthermore, *Nlrp3*-or *Il18*-deficient mice or mice treated with a galectin-3 inhibitor had attenuated isoproterenol (ISO)-induced cardiac inflammation and injury [10,11]. The NLRP3 inflammasome is a key component of the innate immune system response to injury and is activated by excessive levels of reactive oxygen species (ROS), including mitochondrial ROS, among other stimuli [12]. Myocardial infarction and ischemia/reperfusion injuries also activate the CM NLRP3 inflammasome [13,14]. Chronic cardiac inflammation caused by CM inflammasome activation is also a hallmark of heart failure [15].

NADPH oxidase 4 (NOX4) is abundantly expressed in the heart and is the primary source of ROS in CM mitochondria [16]. The expression/activity of NOX4 is significantly increased by pathological insults such as ischemia [17] and sympathetic stimulation [18] and contributes to mitochondrial ROS generation and myocardial oxidative damage [19]. We previously showed that NOX4-derived ROS contribute to cardiac inflammation and pathologic cardiac remodeling and that *Nox4* deletion or inhibition prevents these adverse outcomes [17]. Increased mitochondrial NOX4 expression impairs mitochondrial function and dynamics, contributing to worsened CM relaxation, increased myocardial passive stiffness, and development of diastolic dysfunction [20]. Nonetheless, the precise mechanisms driving cardiac inflammation and dysfunction in response to sympathetic stress and ROS overproduction remain unclear.

Monocyte mobilization and myocardial macrophage infiltration are hallmarks of cardiac inflammation in mice and humans in response to sympathetic insults [10,21,22]. Activation and proliferation of resident cardiac macrophages and recruitment of bone marrow-derived monocytes were both implicated in myocardial injury inflammatory responses and remodeling [22,23]. Neither the phenotypic changes nor the role of these macrophage populations is known in stress cardiomyopathy pathophysiology.

We hypothesized that NOX4-dependent mitochondrial ROS in CM are critical mediators of sympathetic β-adrenoreceptor overstimulation, triggering NLRP3 inflammasome activation, induction of local cardiac inflammation with resident macrophage mobilization, cardiac fibroblast activation and pathological remodeling with impairment of diastolic function. We utilized wild-type and cardiac-specific *Nox4* knock-out mice ($Nox4^{CM-/-}$) that were administered a single dose of β-adrenomimetic ISO. This study focused on the later stages of cardiomyopathy development. We demonstrate that deletion of *Nox4* genetically or inhibition of NOX4 activity pharmacologically attenuates CM mitochondrial ROS levels and inflammasome activation in response to β-adrenergic overstimulation, resulting in reduced cardiac inflammation and fibrosis and preserved diastolic function.

2. Materials and methods

2.1. Animals

All animal procedures were approved by the University of Michigan Institutional Animal Care and Use Committee in accordance with NIH OLAW policy and Guide for the Care and Use of Laboratory Animals, 8th ed. The $Nox4^{flox/flox}$ mice were generated and described previously by Dr. Junichi Sadoshima (Rutgers New Jersey Medical School, Newark, NJ) [16]. The CM-specific *Nox4* deletion was achieved by crossing $Nox4^{flox/flox}$ and αMHC-Cre mice (B6.FVB-Tg(Myh6-cre)2182 Md/J, The Jackson Laboratory; Bar Harbor, MA) which leads to the deletion of exon 9 and early termination of exon 10 resulting in complete loss of NOX4 function in CM [16]. Littermate male mice were used in all experiments. Mice were housed in ventilated cages at 22 °C with a 12-h light/dark cycle and free access to food and water. Mice were randomly assigned to receive either vehicle or an active compound. The two groups were housed in the same cages to avoid environmental bias and stress from single housing. Isoproterenol (Sigma; St. Louis, MO) at 5 mg/kg was injected intraperitoneally in 4-month-old mice (n = 12) to induce sympathetic stress [10]. GKT137831 (Cayman Chemical; Ann Arbor, MI) was dissolved in 0.5% carboxymethylcellulose, 0.25% Tween-20, and 1% dimethyl sulfoxide and given via oral gavage at 100 mg/kg/day for 7 days [24]. At the end of the study, mice were euthanized with inhaled isoflurane overdose, the hearts were dissected, cleared with PBS, and embedded in O.C.T. compound (Sakura Finetek, Torrance, CA), or used for protein lysates.

2.2. Ventricular CM isolation and culture

CM were isolated as described previously [25]. Mice (4-month-old) were euthanized with inhaled isoflurane overdose, the hearts were dissected, canulated through the aorta, and cleared with perfusion buffer (113 mM NaCl, 4.7 mM KCl, 0.6 mM KH_2PO_4, 0.6 mM Na_2HPO_4, 1.2 mM $MgSO_4$, 5.5 Mm $NaHCO_3$, 5.5 mM $KHCO_3$, 30 mM Taurine, 5.5 mM Glucose and 10 mM HEPES, pH 7.4). Buffer containing collagenase type II and 12 μM $CaCl_2$ was continuously perfused for 10 min at 37 °C for enzymatic digestion. Ventricles were dissected and gently minced followed by mechanical cell dispersion. Cells were transferred into stopping buffer (perfusion buffer with 10% fetal bovine serum) and calcium was re-introduced in steps of 5 min to a final concentration of 1.2 mM. Cells were cultured in Minimum Essential Medium (MEM) supplemented with 5% fetal bovine serum, 125 μM blebbistatin, and antibiotic/antimycotic solution (Thermo Fisher; Waltham, MA) in a 5% CO_2 incubator at 37 °C. The CM phenotype of isolated cells was confirmed with qPCR analysis of *Myh7* and *Tnnt2* expression. Isolated cells were left to adhere overnight and then treated with vehicle or 10 μM isoproterenol and/or 10 μM GKT137831.

2.3. ROS detection

Dissected hearts were embedded in O.C.T. compound and snap-frozen in liquid nitrogen. Ventricular transverse serial sections were cut at 10 μM thickness and analyzed immediately after collection. Ventricular ROS and mitochondrial ROS were detected using DHE and MitoSOX Red, respectively, as described previously [26]. Briefly, ventricular sections were incubated with 10 μM DHE or 5 μM MitoSOX Red (Thermo Fisher) in the presence or absence of 200 U/ml PEG-SOD (Sigma) at 37 °C for 30 min. Fluorescence images were acquired using Nikon Microphot-FX microscope and analyzed using NIH Image J 1.53 (Bethesda, MD). Fluorescence background correction was performed

using PEG-SOD-treated control samples.

Hydrogen peroxide levels in the heart tissue and CM were determined as described [17]. Briefly, dissected heart tissue was incubated with 100 μM, and ventricular CM with 50 μM of Amplex Red solution (Thermo Fisher) in the presence or absence of 200 U/ml PEG-catalase (Sigma) at 37 °C for 30 min. The supernatant was collected, and fluorescence was measured using Spectramax M5 spectrophotometer with 530 nm excitation and 590 nm emission filters (Molecular Devices, Sunnyvale, CA). The H_2O_2 levels were calculated using a standard curve generated with fresh H_2O_2, corrected for background fluorescence, and normalized to the dry tissue weight or CM protein concentration. To measure mitochondrial H_2O_2, ventricular sections were incubated with 50 μM MitoPY1 (Thermo Fisher) in the presence or absence of 200 U/ml PEG-catalase (Sigma) at 37 °C for 30 min. Fluorescence images were acquired using Nikon Microphot-FX microscope and analyzed with NIH Image J 1.53. Control samples incubated with PEG-catalase were used for fluorescence background correction.

2.4. Histology and immunostaining

Frozen heart sections were stained with picro-sirius red using Connective Tissue Stain Kit (Abcam; Waltham, MA) and quantified as previously described [17]. Immunofluorescence analysis was performed as described [27]. Frozen heart sections were fixed in acetone, blocked with normal goat serum, and stained with rabbit NOX4, IL18, POSTN (Abcam), CD11b (Itgam; Abnova; Walnut, CA), and ACTA2 (Sigma) followed by Alexa Fluor 594 goat anti-rabbit IgG (Thermo Fisher). The sections were then stained with Alexa Fluor 488-tagged MYH7 or ATP5G2 (Bioss; Woburn, MA) and mounted with VECTASHIELD PLUS Mounting Medium with DAPI (Vector Laboratories; Burlingame, CA). Images were acquired with Nikon Microphot-FX microscope and analyzed using NIH ImageJ 1.53 in a blinded manner. Antigen-specific fluorescence intensity was determined by integrated density. Antigen-positive cells nuclei were counted as a fraction of the total nuclei number per field of view (FOV) [28].

2.5. Western blot and ELISA analysis

Western blotting was performed as described previously [17]. The primary antibodies used were rabbit NOX1, NOX2, NOX4, CAT, IL18, NLRP3 (Abcam), SOD1, TOMM20 (Thermo Fisher) SOD2, cleaved-CASP1, mouse GAPDH (Cell Signaling Technology; Danvers, MA), and mouse TUBB (Sigma). The secondary antibodies used were goat anti-rabbit IRDye 800CW and goat anti-mouse IRDye 680RD (Li-Cor; Lincoln, NE). Immunoreactive protein bands were imaged and analyzed using Li-Cor Odyssey CLx Infrared Imaging System. Heart protein lysates were tested using ELISA for mouse IL18, IL6, CCL2, and TNFα (Thermo Fisher) in accordance with the manufacturer's protocols. LDH activity detection kits (Sigma) were used to detect lactate dehydrogenase activity in mouse plasma after ISO injection.

2.6. Echocardiography

Echocardiography analysis was performed as described previously [26]. Mice were anesthetized with inhaled 1% isoflurane/O_2 mixture and fixed on the temperature-controlled ECG board. Ultrasound M-mode, pulsed-wave, and tissue Doppler mode images were acquired with Vevo 2100 high-resolution micro-imaging system equipped with a 22–55 MHz MicroScan transducer (FUJIFILM Visual Sonics; Toronto, ON). Measurements of cardiac function parameters were derived using Vevo 2100 software.

2.7. Invasive left ventricle pressure-volume analysis

LV pressure-volume analysis was performed as described [20]. Mice were anesthetized with an inhaled 1% isoflurane/O_2 mixture and placed in the supine position on the temperature-controlled ECG board. Apex of the heart was exposed through thoracotomy and apical stab was made with 27G needle. A 1.2F pressure-volume catheter (FTH-1212B-4518, Transonic; Ithaca, NY) was inserted through the stab wound and pressure-volume loops were recorded at 1000Hz with ADV500/AD-Vantage system (Transonic). A baseline scan was performed to record load-dependent values, then inferior vena cava was occluded to derive load-independent indices. Data were analyzed with LabScribe v2 software (iWorx; Dover, NH).

2.8. Flow cytometry analysis

Whole blood was collected in Heparin-containing tubes from deeply anesthetized mice through cardiac puncture. Red blood cells were lysed using 1x RBC lysis buffer (Thermo Fisher), the remaining cellular fractions were washed with PBS and passed through a 70 μm cell strainer (Corning; Corning, NY). Cells were blocked with rat anti-mouse CD16/CD32 antibodies (BD Biosciences; Franklin Lakes, NJ) and stained with APC-conjugated anti-CD11b (Miltenyi Biotec; Gaithersburg, MD), PE/Cy7-conjugated anti-CD115 (Biolegend; San Diego, CA) and FITC-conjugated *anti*-LY6C (Miltenyi Biotec) antibodies. The samples were fixed using Foxp3/Transcription Factor Staining Buffer Set (eBioscience). Data were acquired with MoFlo Astrios EQ Cell Sorter (Beckman Coulter) and analyzed with FlowJo 10 (FlowJo LCC). Peripheral blood monocytes were identified as $CD11b^+CD115^+Ly6C^+$ fraction of all analyzed cells.

2.9. Spectral flow cytometry analysis

A multi-color flow cytometry antibody panel was designed using FluoroFinder (Broomfield, CO). Antibody fluorochrome tags were selected based on their spectral characteristics, ensuring the unique full-spectrum signature and minimal fluorescence spillover (Supplemental Table 1).

Single-cell suspension for flow cytometry analysis was prepared as previously described [27]. Briefly, mice were euthanized with inhaled isoflurane overdose, the hearts were dissected and cleared with PBS. Ventricles were dissected and gently minced followed by enzymatic digestion in collagenase type I 450 U/ml, collagenase type XI 125 U/ml and hyaluronidase 60 U/ml solution. Cell suspension was passed through a 70 μm cell strainer (Corning; Corning, NY) and washed in FACS buffer (PBS, 1% BSA, 1 mM EDTA). Samples were centrifuged at 400×*g* for 5 min at 4 °C and the supernatant was discarded. The pellets were resuspended in 200 μl PBS containing 1:1000 Ghost Dye Red 710 for live/dead staining, 1:100 anti-mouse CD16/32 antibodies (BioLegend) to block Fc receptor and incubated for 30 min at 4 °C protected from light. The samples were washed with PBS, centrifuged, and resuspended with 200 μL FACS buffer with cell surface marker antibody mix (Supplemental Table 1). Samples were incubated for 60 min at 4 °C and washed in PBS. The samples were fixed and permeabilized using Foxp3/Transcription Factor Staining Buffer Set (eBioscience) in accordance with manufacturer's protocol. Samples were then resuspended in 200 μL permeabilization buffer containing intracellular marker antibody mix (Supplemental Table 1), incubated for 45 min protected from light washed sequentially in permeabilization buffer and in FACS buffer then resuspended in 300 μl of FACS buffer. Flow cytometry analysis was performed with Aurora Spectral Analyzer (Cytek; Freemont, CA). Instrument setup and quality controls were performed prior to acquisition according to the manufacturer's protocol. UltraComp Beads (Invitrogen) bound with corresponding antibodies (Supplemental Table 1) were used as single-stained controls. An unmixing matrix with autofluorescence extraction was calculated using SpectroFlo software (Cytek) and the multicolor-targeted samples were run using the live unmixing. The same reference controls were used for unmixing of multiple experiments and all samples were run within 1 week.

Unmixed fcs files were concatenated and analyzed using FCS Express

7 (DeNovo software). Biexponential transformation was set to ensure all events were displayed within the axes. Manual gating was used to target macrophages or fibroblasts specifically (Supplemental Figs. 1 and 2). The following parameters were used for dimensionality reduction: down-sampling algorithm was set to weighted density with 100000 events sample size, Barnes-Hut approximation was set at 0.03 and the perplexity at 80. Opt-SNE algorithm was used with 2500 iterations. Differentially enriched t-SNE clusters were manually gated and gating heat maps with macrophage- or fibroblast-corresponding antibody parameters were created. The gate-specific statistical analysis was performed in FCS Express 7.

2.10. Apoptosis and necrosis assessment

Apoptosis in heart cells was determined by flow cytometry using FITC Annexin V Dead Cell Apoptosis Kit (Thermo Fisher). Single-cell suspension was prepared as described above. The samples were washed with FACS buffer (PBS, 1% BSA, 1 mM EDTA) and stained with propidium iodide and FITC-conjugated annexin V antibody according to the manufacturer's protocol. The samples were run on Aurora Spectral Analyzer (Cytek), and data were analyzed with FlowJo v10 (FlowJo, Stanford University, CA). Each sample was assessed for the percentage of propidium iodide-positive dead cells and annexin V-positive/propidium iodide-negative cells undergoing apoptosis.

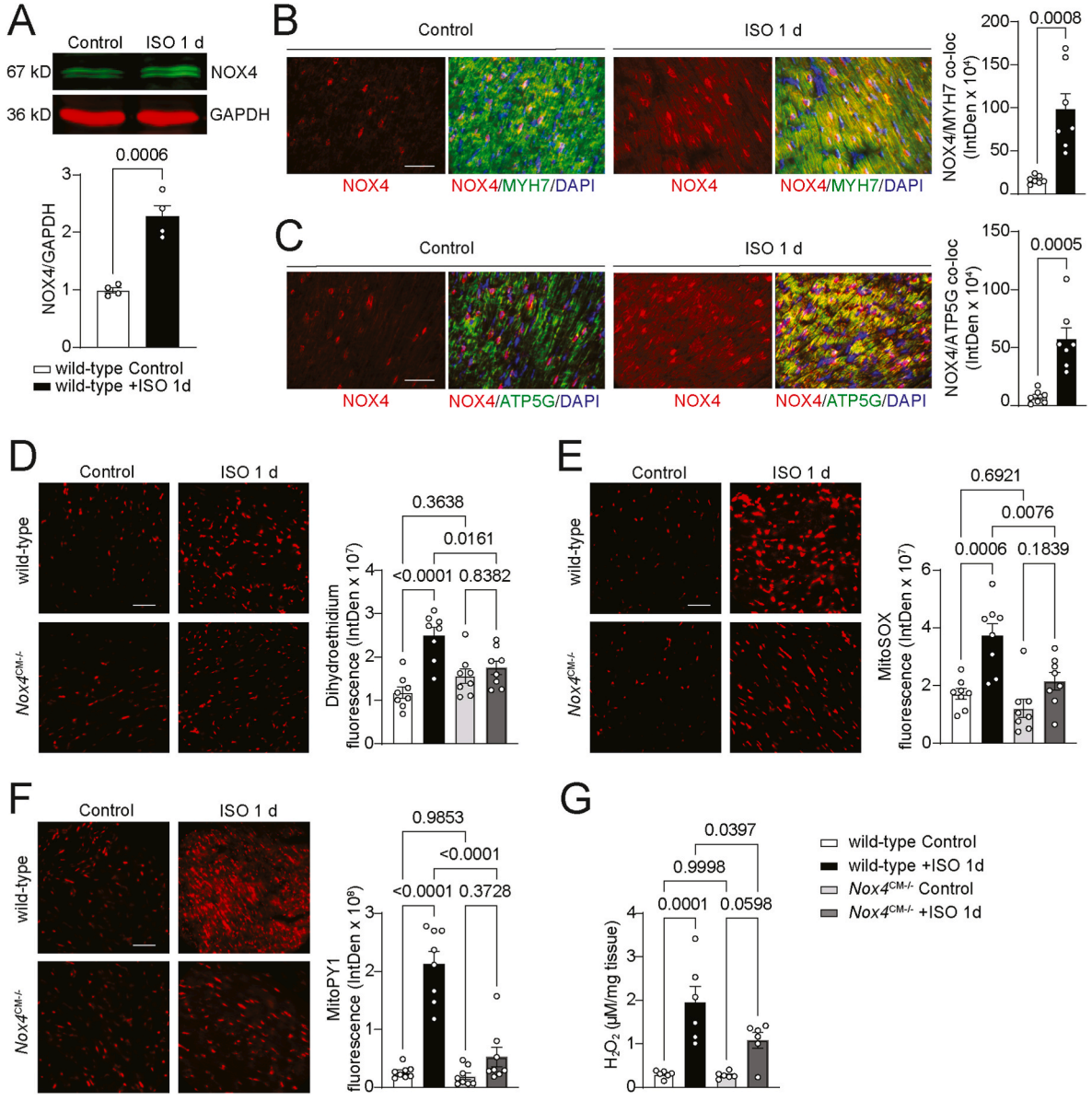

Fig. 1. ISO treatment induces NOX4-dependent mitochondrial oxidative stress in the heart.
(A) Western blot analysis and quantification of NOX4 expression in the protein lysates from wild-type mice hearts 1 day after treatment with vehicle or 5 mg/kg ISO. Data are mean ± SEM (n = 4) of NOX4 expression fold change adjusted for GAPDH levels relative to wild-type control. **(B–C)** Representative fluorescence microscopy images and quantification of NOX4 colocalization with CM (MYH7 **(B)** and mitochondrial (ATP5G **(C)** markers in the transverse left ventricle sections from wild-type mice 1 day after treatment with vehicle or ISO stained for immunoreactive NOX4 (red), MYH7 or ATP5G (green), and DAPI (blue). Data are fluorescence integrated density (mean ± SEM, n = 7). **(D–F)** Representative fluorescence microscopy images and quantification of DHE **(D)**, MitoSOX **(E)**, and MitoPY **(F)** fluorescence in the transverse left ventricle sections from wild-type and *Nox4*$^{CM-/-}$ mice 1 day after treatment with vehicle or ISO. Data are fluorescence integrated density (mean ± SEM, n = 8). **(G)** Hydrogen peroxide levels were measured using AmplexRed assay in the heart samples from wild-type and *Nox4*$^{CM-/-}$ mice 1 day after treatment with vehicle or ISO (mean ± SEM, n = 6). Scale is 100 μm.

2.11. Statistics

All analyses were performed using Prism 9 (GraphPad; La Jolla, CA). All data sets were tested for normality using the Shapiro-Wilk test. Data were analyzed using unpaired *t*-test or one-way ANOVA followed by Tukey's multiple comparisons tests, where appropriate. Differences were considered significant at $P < 0.05$.

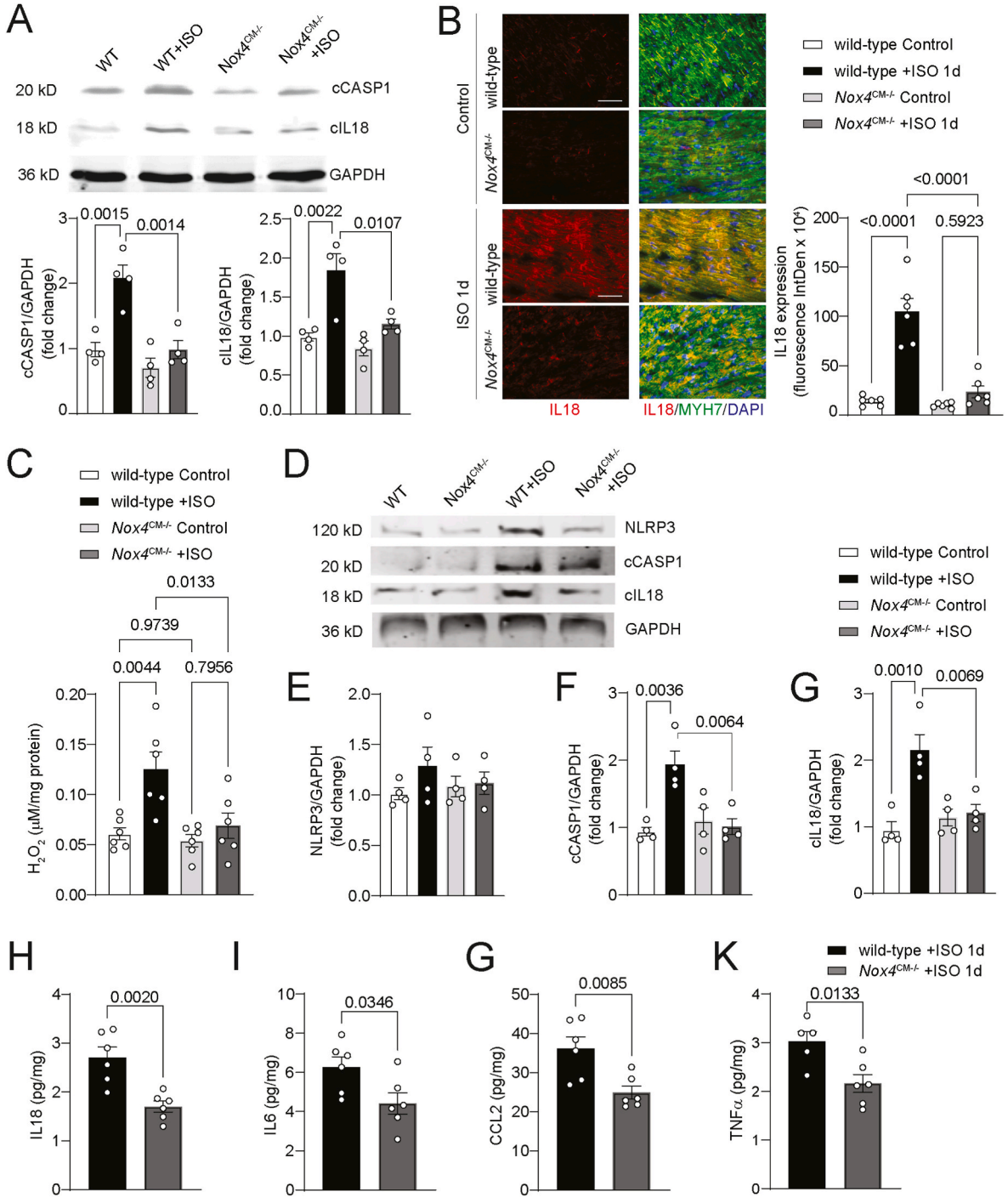

Fig. 2. *Nox4* deletion reduces ISO-induced inflammasome activation in CM.
(A) Western blot analysis of cleaved caspase 1 and IL18 levels in the protein lysates from wild-type and *Nox4*$^{CM-/-}$ mice 1 day after treatment with ISO. Data are fluorescence intensity fold change over wild-type control adjusted for GAPDH levels (mean ± SEM, n = 4). **(B)** Representative fluorescence microscopy images and quantification of IL18 expression in the transverse left ventricle sections from wild-type and *Nox4*$^{CM-/-}$ mice 1 day after treatment with vehicle or ISO stained for immunoreactive IL (red), MYH7 (green), and DAPI (blue). Data are fluorescence integrated density (mean ± SEM, n = 6). Scale is 100 μm. **(C)** Hydrogen peroxide levels were measured using AmplexRed assay in the cultured CM isolated from wild-type and *Nox4*$^{CM-/-}$ mice and treated with ISO (mean ± SEM, n = 6). **(D–G)** Western blot analysis **(D)** and densitometric quantification of NLRP3 **(E)**, cleaved caspase 1 **(F)**, and cleaved IL18 **(G)** expression levels in isolated CM from wild-type and *Nox4*$^{CM-/-}$ mice treated with ISO for 3 h. Data are protein expression fold change relative to vehicle-treated wild-type CM and adjusted for GAPDH levels (mean ± SEM, n = 4). **(H–K)** ELISA analysis of IL18 **(H)**, IL6 **(I)**, CCL2 **(J)**, and TNFα **(K)** levels in the heart protein lysates from wild-type and *Nox4*$^{CM-/-}$ mice 1 day after treatment with ISO (mean ± SEM, n = 6).

3. Results

ISO treatment induces cellular and mitochondrial oxidative stress in wild-type but not in Nox4-deficient CM. To assess the effects of β-adrenergic overstimulation on CM mitochondrial oxidative stress and ROS levels, we first determined NOX4 expression levels in the heart 1 day after ISO treatment. Western blot analysis of heart protein lysates showed that NOX4 expression was significantly increased in wild-type mice (2.2-fold; Fig. 1A). Similarly, NOX4 expression determined by immunofluorescence staining of frozen LV sections from wild-type mice increased significantly in CM after ISO treatment (5.8-fold; Fig. 1B). Because CM NOX4 is primarily localized in mitochondria [19], we also determined the colocalization of immunoreactive NOX4 with the mitochondrial marker ATP5G in LV sections from wild-type mice. In ISO-treated animals, mitochondrial NOX4 expression was 9.1-fold higher than in control animals (Fig. 1C). Further, we assessed the expression levels of other NOX catalytic subunits - NOX1 and NOX2 and ROS-scavenging enzymes - SOD1, SOD2, and CAT in the heart protein lysates of control and ISO-treated wild-type or *Nox4*$^{CM-/-}$ mice. Our assessment showed no significant differences between the two groups (Supplemental Fig. 1).

Measurement of cellular superoxide levels in the frozen LV sections showed significantly increased dihydroethidium fluorescence after ISO treatment in the wild-type but not in *Nox4*$^{CM-/-}$ mice (1.9- and 1.1-fold, respectively; Fig. 1D). Furthermore, mitochondrial superoxide levels determined by MitoSOX fluorescence significantly increased in ISO-treated wild-type heart sections but not in those from *Nox4*-deficient hearts (2.2- vs. 1.7-fold, respectively; Fig. 1E). Because NOX4 primarily generates hydrogen peroxide (H_2O_2) [29], we used MitoPY1 fluorescence to quantify mitochondrial H_2O_2 levels in LV sections. Consistent with increased mitochondrial NOX4 levels in the heart after ISO treatment (Fig. 1C), MitoPY1 fluorescence significantly increased in wild-type but not in *Nox4*-deficient CM (9.2- vs. 4.5-fold, respectively; Fig. 1F). Congruent with that, ISO-induced H_2O_2 levels in the heart measured with Amplex Red assay were significantly higher in wild-type than in *Nox4*$^{CM-/-}$ mice (6.5- vs. 3.8-fold, respectively; Fig. 1G). The expression levels of mitochondrial marker TOMM20 in heart protein lysates did not differ significantly between wild-type and *Nox4*$^{CM-/-}$ mice treated with either vehicle or ISO (Supplemental Fig. 2), indicating no ISO-induced changes in mitochondrial mass. These findings suggest that ISO treatment significantly increases myocardial mitochondrial NOX4 expression, resulting in an increase in H_2O_2 and mitochondrial ROS levels.

CM-specific Nox4 deletion reduces ISO-induced inflammasome activation and cytokine levels. Excessive mitochondrial ROS can directly activate the NLRP3 inflammasome [12]. We previously showed that ISO treatment activates CM inflammasome and releases IL18 [10]. Consistent with that observation, Western blot analysis of protein lysates from ISO-treated wild-type hearts showed significantly higher levels of cleaved caspase 1 (cCASP1) and IL18, which were attenuated in *Nox4*-deficient hearts (Fig. 2A). Accordingly, ISO treatment significantly increased immunoreactive IL18 expression in LV CMs of wild-type mice, whereas no change in IL18 expression was observed in CMs of *Nox4*$^{CM-/-}$ mice, as demonstrated by immunofluorescence co-staining for MYH7 (8- vs. 2.9-fold, respectively; Fig. 2B).

To test whether CM β-adrenoreceptor-dependent inflammasome activation is mediated by NOX4-dependent mitochondrial oxidative stress, we treated CM isolated from wild-type or cardiac *Nox4*-deficient mice with ISO. Using the Amplex Red assay, we first demonstrated that ISO treatment significantly increased H_2O_2 generation in cultured wild-type CM by 2-fold but not in *Nox4*-deficient CM (1.3-fold increase; Fig. 2C). Western blot analysis revealed that ISO treatment did not affect NLRP3 inflammasome expression levels (Fig. 2D–E). However, inflammasome activity was significantly increased as determined by a 1.75-fold increase in cleaved caspase 1 (cCASP1) and a 2-fold increase in IL18 after ISO treatment (Fig. 2D–G). CMs lacking *Nox4* did not show a significant increase in inflammasome activation after ISO treatment.

Additionally, ELISA analysis of heart protein lysates from ISO-treated wild-type mice showed significantly higher levels of IL18, IL6, CCL2, and TNFα cytokines than in *Nox4*$^{CM-/-}$ mice (Fig. 2H–K). The cytokine levels in control mouse hearts were below the assay detection level. These results confirm our previous observations of ISO-induced heart inflammasome activation and suggest that NOX4 is a critical upstream regulator of mitochondrial ROS-induced NLRP3 inflammasome activation and inflammation initiation in the heart.

NOX4 regulates adrenergic overstimulation-induced expansion of embryonic-derived resident macrophage populations in the heart. ISO induces macrophage infiltration in the heart in an inflammasome/IL18-dependent manner [10]. In line with that, immunofluorescent staining of LV sections showed that wild-type hearts had significantly more CD11b$^+$ macrophages than *Nox4*-deficient hearts 3 days after ISO treatment ($P < 0.01$; Fig. 3A). Similarly, CD68$^+$ immunofluorescence in the LV of wild-type but not of *Nox4*$^{CM-/-}$ mice was significantly increased after ISO treatment ($P < 0.001$; Fig. 3B). To assess whether bone marrow-derived monocyte mobilization affects cardiac macrophage numbers, we performed flow cytometry analysis of peripheral blood cells from wild-type and *Nox4*$^{CM-/-}$ mice before and 1 day after ISO treatment. There were no significant differences in the proportion of peripheral CD115$^+$ monocytes between control wild-type and *Nox4*$^{CM-/-}$ mice and ISO treatment did not induce a significant increase in monocyte numbers. Similarly, the proportion of Ly6C^{hi}CD115$^+$ and Ly6C^{lo}CD115$^+$ monocytes in wild-type and *Nox4*$^{CM-/-}$ mice were unaffected by ISO treatment (Fig. 3C), suggesting that ISO treatment did not mobilize pro-inflammatory monocytes.

To better understand the mechanisms of ISO-induced macrophage infiltration into the heart, we performed spectral flow cytometry analysis of heart single-cell suspensions. First, we analyzed the proportion of macrophages in the LV samples from wild-type and *Nox4*$^{CM-/-}$ mice before and 3 days after ISO treatment. The proportion of macrophages in control wild-type and *Nox4*-deficient hearts did not differ significantly. However, wild-type mice had a significantly higher proportion of CD68$^+$CD11b$^+$ cells as a percent of all heart cells after ISO treatment (2.5-fold increase, $P < 0.01$; Fig. 3D). In contrast, ISO treatment had no significant effect on the proportion of these cells in *Nox4*$^{CM-/-}$ mice.

Because recruited monocyte-derived as well as embryonic-derived resident heart macrophages may contribute to an increased number of infiltrating inflammatory cells [30], unbiased multidimensional flow cytometry t-Distributed Stochastic Neighbor Embedding (t-SNE) analysis was performed to identify specific macrophage subsets. A t-SNE analysis combines all parameters of a single cell into a two-dimensional map by clustering the cells with similar properties. To increase the specificity of the analysis, all live cells were negatively gated for ACTA2 and CD3 to select CD11b$^+$CD68$^+$ cells (Supplemental Fig. 3). We identified 8 distinct clusters whose enrichment changed with ISO treatment based on the expression of LY6C, CCR2, CX3CR1, MKI67, TNFα, IL6, TGFβ, MHCII, and LGALS3 (Fig. 3E–G). Congruent to our observation of no increase in inflammatory Ly6C^{hi} monocytes in the peripheral blood after ISO treatment (Fig. 3C), none of the clusters contained classic recruited monocyte-derived pro-inflammatory macrophages (Fig. 3G).

Non-classical recruited monocyte-derived tissue repair macrophages (CCR2$^+$CX3CR1$^+$Ly6C^{lo}) [31] were present in clusters 1, 7, and 8 (Fig. 3G). Cluster 1 was significantly enriched in wild-type but not *Nox4*-deficient hearts after ISO treatment and had increased expression of LGALS3, an inflammatory and pro-fibrotic macrophage marker [11] (Fig. 3H). Wild-type hearts did not show any significant changes in clusters 7 or 8, whereas knockout hearts showed a decrease in cluster 7 and an increase in cluster 8, supported by lower or higher expression of proliferation marker MKI67, respectively.

The remaining clusters 2–6 were mainly composed of embryonic-derived resident heart macrophages (CCR2$^-$MHCII$^+$) [32]. Clusters 2 and 3 were significantly enriched after ISO treatment in wild-type but were depleted in *Nox4*$^{CM-/-}$ mice. These clusters were characterized by resident macrophages (CCR2$^-$MHCII^{hi}CX3CR1^{hi}) expressing

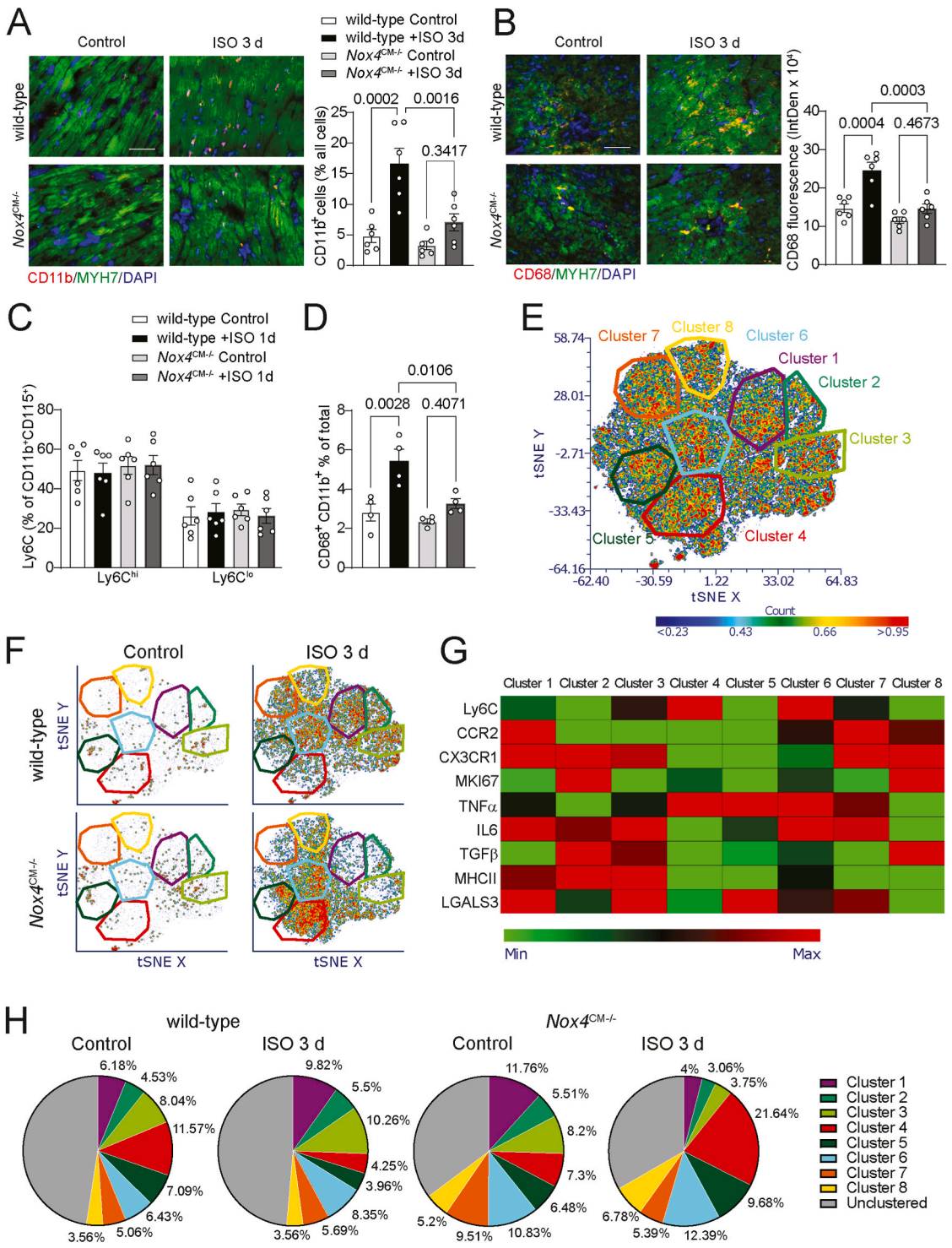

Fig. 3. Multidimensional flow cytometry analysis of changes in macrophage subpopulations in the hearts after ISO treatment.
(A) Representative fluorescence microscopy images and quantification of CD11b$^+$ cells in the transverse left ventricle sections from wild-type and *Nox4*$^{CM-/-}$ mice 3 days after treatment with ISO stained for immunoreactive CD11b (red), MYH7 (green), and DAPI (blue). Data are fraction of CD11b$^+$ cells as a percent of all cells in the FOV (mean ± SEM, n = 6). Scale is 100 μm. **(B)** Representative fluorescence microscopy images and quantification of CD68$^+$ fluorescence in the left ventricle sections stained for immunoreactive CD68 (red), MYH7 (green), and DAPI (blue). Data are fluorescence integrated density adjusted for the number of cells in the FOV (mean ± SEM, n = 6). Scale is 100 μm. **(C)** Flow cytometry analysis of peripheral blood CD11b$^+$CD115$^+$Ly6C$^+$ monocytes in wild-type and *Nox4*$^{CM-/-}$ mice 1 day after treatment with vehicle or ISO. Data are Ly6C$^+$ cells as a percent of CD11b$^+$CD115$^+$ cells (mean ± SEM, n = 6). **(D)** Flow cytometry analysis of LV single cell suspension for infiltrating macrophages. Data are a fraction of CD68$^+$CD11b$^+$ cells as a percent of all LV cells (mean ± SEM, n = 4). **(E)** t-SNE analysis of heart flow cytometry data from wild-type and *Nox4*$^{CM-/-}$ mice 3 days after treatment with vehicle or ISO. CD68$^+$CD11b$^+$ cells (n = 100,000) were clustered based on the expression of CCR2, CX3CR1, IL6, LY6C, MHCII, MKI67, TNFα, TGFβ, and LGALS3. Distinct clusters were projected over t-SNE plot. **(F)** t-SNE clustering and identification of cardiac macrophage clusters in the control and ISO-treated wild-type and *Nox4*$^{CM-/-}$ mice (n = 4). **(G)** Heat map representation of macrophage markers relative mean fluorescence intensity for each distinct cluster. **(H)** Relative enrichment of cardiac macrophage clusters as a proportion of cells from the control and ISO-treated wild-type and *Nox4*$^{CM-/-}$ mice used in t-SNE analysis.

pro-fibrotic cytokines - TGFβ and IL6. In addition, cluster 2 showed higher expression of MKI67 whereas cluster 3 higher expression of Ly6C and LGALS3 suggesting that cells in cluster 2 are actively expanding and acquiring pro-inflammatory and pro-fibrotic characteristics, enriching cluster 3. Clusters 4, 5, and 6 composed of resident repair macrophages ($CCR2^{-}MHCII^{lo}CX3CR1^{lo}$) and were enriched in ISO-treated *Nox4*-deficient hearts, unlike wild-type mice where they were depleted. Cells in these clusters did not express any inflammatory or pro-fibrotic markers except TNFα. Their expression of Ly6C indicates that they may have evolved from pro-inflammatory cells. In summary, sympathetic stress-induced CM inflammation increased embryonic-derived resident pro-fibrotic macrophage populations. In contrast, CM *Nox4* deletion and attenuation of inflammation significantly reduced pro-inflammatory macrophage subpopulations and increased tissue repair macrophage subpopulations with limited pro-fibrotic activity.

The activation and differentiation of cardiac fibroblasts are attenuated in $Nox4^{CM-/-}$ *mice.* An increase in macrophage infiltration in the heart results in an inflammatory and pro-fibrotic environment that activates resident cardiac fibroblasts [33]. Therefore, we assessed cardiac fibroblast phenotype using flow cytometry t-SNE analysis in wild-type and $Nox4^{CM-/-}$ hearts 3 days after ISO injection. All analyzed live cells were negatively gated for CD31 and CD3, and positively gated for FAP (Supplemental Fig. 4). The proportion of FAP^{+} fibroblasts in the hearts of wild-type and $Nox4^{CM-/-}$ mice was not significantly different before or after ISO treatment (Fig. 4A). Based on the expression of ACTA2, COL1A1, MKI67, CD90, and TGFβ, the analysis revealed 7 distinct clusters of cardiac fibroblast subpopulations that were either enriched or depleted after ISO treatment (Fig. 4B–D).

ISO treatment highly enriched clusters 5 and 7 that consisted of the cardiac fibroblasts with high expression of proliferation marker MKI67 (Fig. 4D and E). Cells in clusters 1 and 3 showed no greater enrichment after ISO treatment in both genotypes and were low in anchoring protein CD90, indicating migratory activity. Also, these fibroblasts expressed more TGFβ. Cluster 2 was characterized by anchored collagen-secreting myofibroblasts with high expression of ACTA2, COL1A1, and CD90 proteins. Both genotypes showed relative depletion of this cluster after ISO treatment. Clusters 4 and 6 were represented by proto-myofibroblasts with low expression of ACTA2 [34].

The most prominent differences were observed in cluster 6 which was enriched in wild-type but depleted in $Nox4^{CM-/-}$ hearts. The fibroblasts in this cluster had high expression of collagen I (COL1A1) and low expression of CD90. Cluster 4 consisted of cells expressing COL1A1 and CD90 but were not changed in either genotype following ISO treatment. These results demonstrate that pro-fibrotic activation of cardiac macrophages causes dynamic changes in heart fibroblast populations. Specifically, activated fibroblast proliferation and migration along with increased collagen-producing myofibroblasts were observed in wild-type hearts. Activated fibroblasts in *Nox4*-deficient hearts, however, did not increase myofibroblast numbers.

We further investigated the changes in activated cardiac fibroblasts and myofibroblasts following seven days of ISO treatment [35,36]. In LV cross sections from wild-type mice, non-myocyte $POSTN^{+}$ cells were 6.5-fold more abundant than in sections from vehicle-treated mice (Fig. 4F). In the heart sections from $Nox4^{CM-/-}$ mice, non-myocyte $POSTN^{+}$ cells were significantly less abundant than those from wild-type mice 7 days after ISO treatment. Additionally, a 3-fold increase in the percentage of $ACTA2^{+}$ non-myocytes was observed 7 days after ISO treatment in wild-type compared with *Nox4*-deficient hearts (Fig. 4G). These results support the notion that mitochondrial ROS-induced CM inflammation activates IL6-and TNFα-secreting pro-fibrotic resident macrophages, which in turn increases the expansion of activated and myofibroblast populations in the heart.

CM-specific Nox4 deletion attenuates sympathetic stress-induced heart interstitial fibrosis and diastolic dysfunction. Cardiac myofibroblasts are the primary mediators of fibrosis in the heart [37] and our previous study showed significantly increased interstitial fibrosis and impaired diastolic function in the hearts seven days after ISO treatment [10]. In line with that, picrosirius-positive interstitial collagen deposition was significantly increased in the LV cross sections from ISO-treated wild-type mice (Fig. 5A). In contrast, the ISO-induced picrosirius-positive area in LV sections from $Nox4^{CM-/-}$ mice was significantly lower. Flow cytometry analysis of propidium iodide (PI)-positive dead cells and annexin V (ANXA5)-positive apoptotic cells from vehicle- or ISO-treated mice did not show measurable induction of CM necrosis or apoptosis in wild-type or *Nox4*-deficient hearts (Supplemental Fig. 5A; Fig. 5B). In addition, plasma LDH levels (a marker of myocardial damage) did not change 1, 3, or 7 days after ISO treatment (Supplemental Fig. 5B). Hence, interstitial collagen deposition observed in ISO-treated mice cannot be attributed to replacement fibrosis in response to CM apoptosis or necrosis.

Excessive interstitial collagen deposition in the heart reduces myocardial compliance and impairs relaxation during diastole [20]. Sympathetic overstimulation did not alter heart weight, suggesting that wild-type or $Nox4^{CM-/-}$ mice do not have hypertrophic responses or systolic function deficits (Fig. 5C). We further evaluated heart function in these mice using pulsed-wave and tissue Doppler echocardiography (Fig. 5D). Left ventricle ejection fraction and end-diastolic volume did not change significantly, supporting the notion of preserved systolic function (Fig. 5E–F). In contrast, diastolic function assessment revealed an increase in the early diastolic mitral valve flow peak E-wave velocity and a decrease of mitral valve septal annulus E′-wave velocity, as well as an increase of E/E′ ratio predicting increased LV filling pressure in ISO-treated wild-type mice, but not in ISO-treated cardiac *Nox4*-deficient mice (Fig. 5G–I). Furthermore, ISO-treated wild-type mice showed significantly shorter mitral valve E-wave deceleration times than *Nox4*-deficient mice (Fig. 5J), suggesting decreased LV compliance. In addition, invasive hemodynamic assessment using pressure-volume relationship analysis also showed no changes in ejection fraction after ISO treatment. LV end-diastolic pressure, pressure-volume relationship, and minimum rate of diastolic pressure decay were significantly increased in wild-type mice after ISO treatment compared to that in $Nox4^{CM-/-}$ mice (Fig. 5K-N), suggesting increased LV wall stiffness. As there were no significant changes in the isovolumic relaxation time and time constant for isovolumic relaxation (Supplemental Fig. 6), our results do not support the hypothesis that ISO treatment induces changes in CM relaxation [38]. These observations showed that sympathetic overstimulation can lead to restrictive diastolic dysfunction, impaired LV compliance, and increased filling pressure, which may be mediated by CM NOX4 activation, mitochondrial oxidative stress, and inflammation.

Pharmacological inhibition of NOX4 attenuates sympathetic stress-induced cardiac diastolic dysfunction. To test whether CM β-adrenoreceptor-induced inflammasome activation is mediated by NOX4-dependent mitochondrial oxidative stress, wild-type mouse neonatal CM were treated with ISO and with or without NOX4/NOX1 inhibitor GKT137831, previously shown to reduce NOX4-dependent mitochondrial ROS and inflammation in the murine cardiovascular system [26]. Western blot analysis of NLRP3 expression did not reveal significant changes (Fig. 6A and B). In contrast, ISO treatment-induced inflammasome activity was attenuated by pretreatment with GKT137831, as shown by decreased levels of cCASP1 (Fig. 6A and C) and cIL18 (Fig. 6A and D). These findings show that NOX4-dependent mitochondrial ROS are critical for ISO-induced NLRP3 inflammasome activation.

To determine whether pharmacological targeting of NOX4-dependent mitochondrial oxidative stress attenuates diastolic dysfunction, ISO-injected mice were treated with GKT137831. MitoSOX fluorescence measurements in heart cross sections of ISO-injected mice treated with GKT137831 for 3 days showed a significant reduction in mitochondrial superoxide levels (Fig. 6E). As expected, heart mitochondrial H_2O_2 levels were also significantly lower in GKT-treated mice, as determined by MitoPY1 fluorescence (Fig. 6F).

Analysis of LV sections from mice 3 days after ISO treatment showed

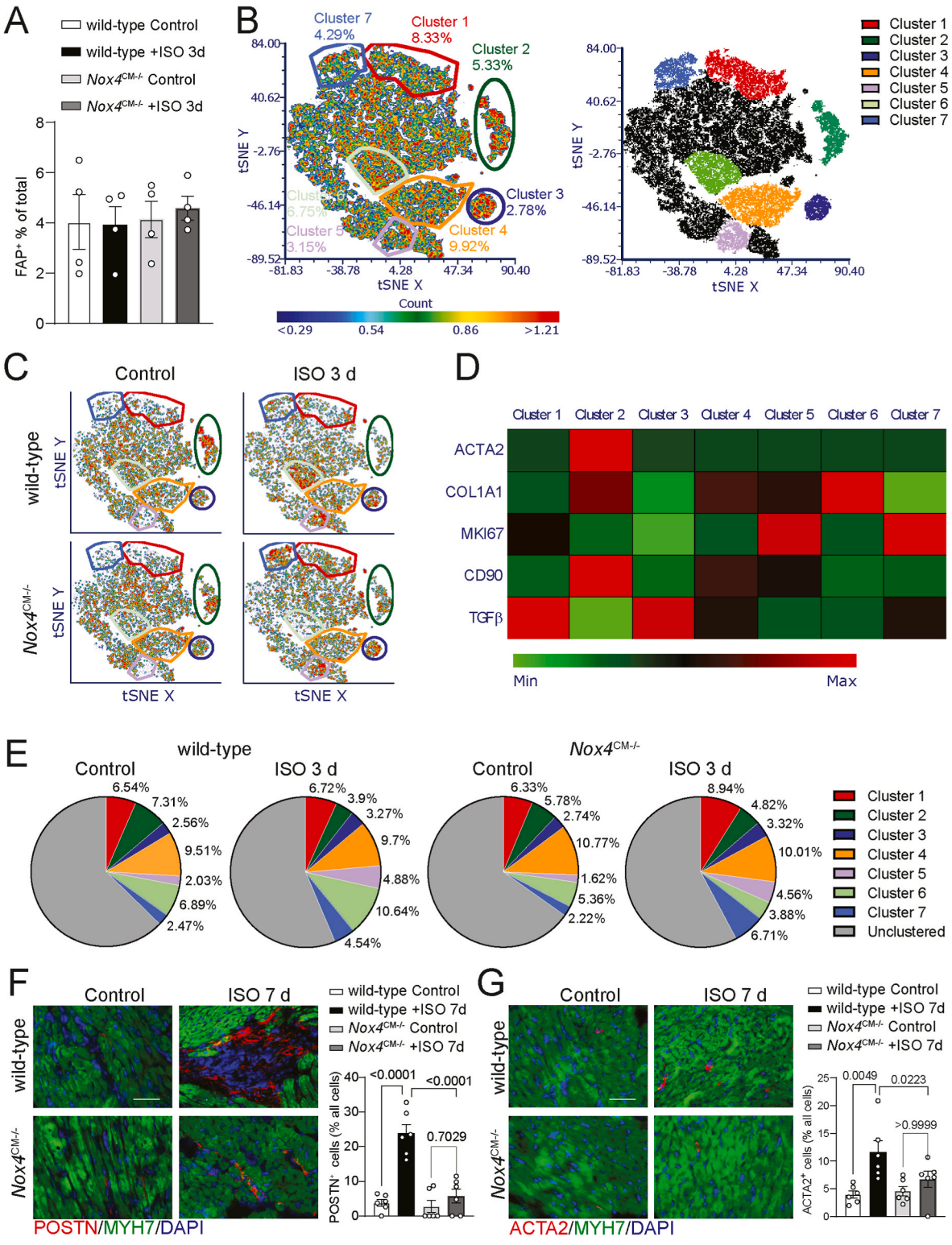

Fig. 4. ISO-induced cardiac fibroblasts activation is reduced in *Nox4*$^{CM-/-}$ mice.
(A) Flow cytometry analysis of LV single cell suspension for cardiac fibroblasts. Data are a fraction of FAP$^+$ cells as a percent of all LV cells (mean ± SEM, n = 4). **(B)** t-SNE analysis of flow cytometry data from CD31$^-$CD3$^-$FAP$^+$ heart cells suspension (n = 100,000) from wild-type and *Nox4*$^{CM-/-}$ mice 3 days after treatment with vehicle or ISO. Cells were clustered based on the expression of TNFα, TGFβ, IL10, MKI67, ACTA2, and COL1A1. Distinct clusters were projected over t-SNE plot (right panel). **(C)** t-SNE clustering and identification of cardiac fibroblast clusters in the control and ISO-treated wild-type and *Nox4*$^{CM-/-}$ mice (n = 4). **(D)** Heat map representation of fibroblast markers relative expression for each distinct cluster. **(E)** Relative enrichment of cardiac fibroblast clusters as a proportion of cells from the control and ISO-treated wild-type and *Nox4*$^{CM-/-}$ mice used in t-SNE analysis. **(F)** Representative fluorescence microscopy images and quantification of POSTN$^+$ cells in the transverse left ventricle sections from wild-type and *Nox4*$^{CM-/-}$ mice 7 days after treatment with ISO stained for immunoreactive POSTN (red), MYH7 (green), and DAPI (blue). Data are a fraction of POSTN$^+$ cells as a percent of all cells in the FOV (mean ± SEM, n = 6). **(G)** Representative fluorescence microscopy images and quantification of ACTA2$^+$ cells in the transverse left ventricle sections from wild-type and *Nox4*$^{CM-/-}$ mice 3 days after treatment with ISO stained for immunoreactive ACTA2 (red), MYH7(green), and DAPI (blue). Data are a fraction of ACTA2$^+$ cells as a percent of all cells in the FOV (mean ± SEM, n = 6). Scale is 100 μm.

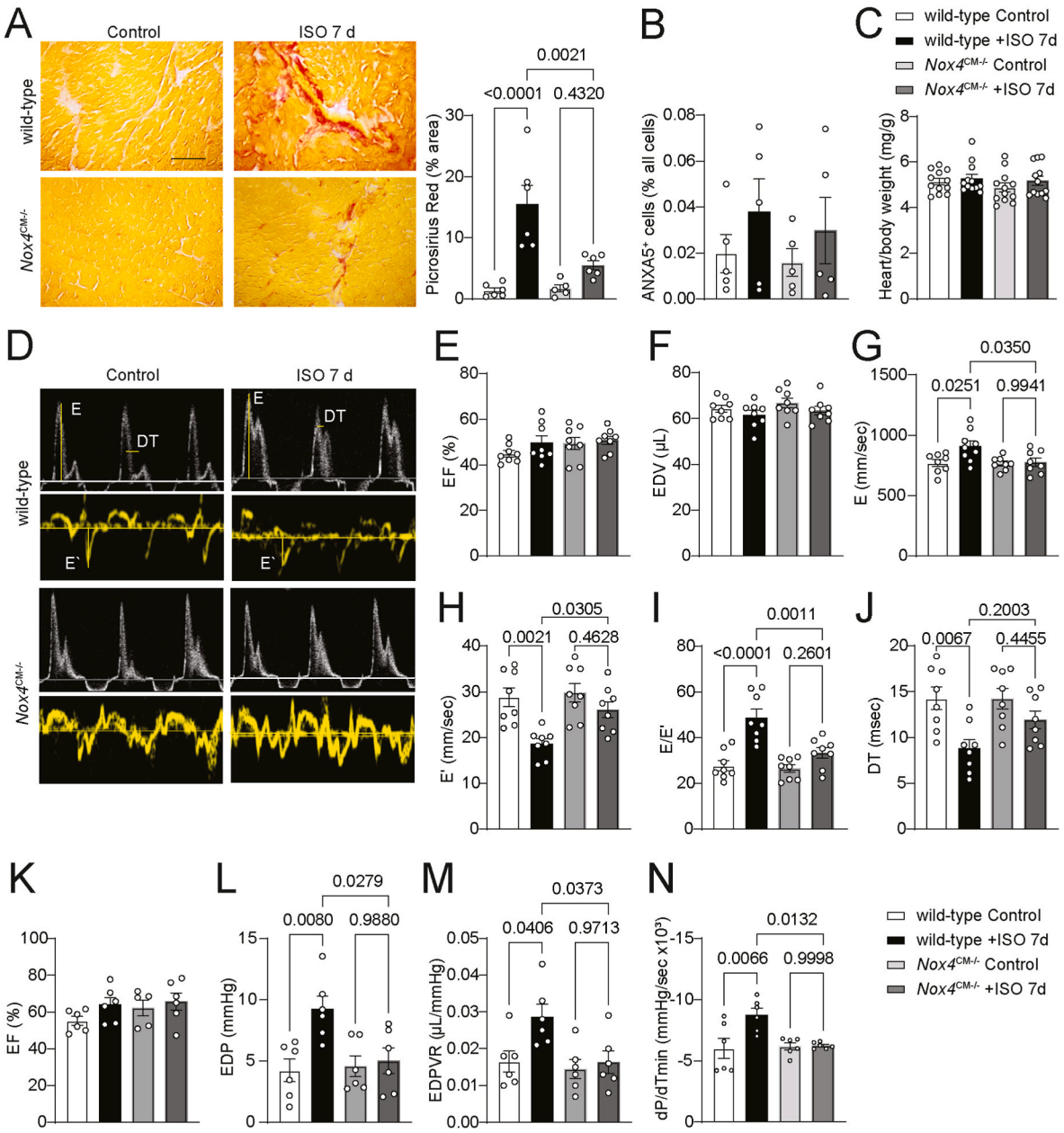

Fig. 5. CM *Nox4* deletion attenuates interstitial fibrosis and preserves diastolic function in ISO-treated mice.
(A) Representative microscopy images and quantification of picrosirius red staining in the transverse left ventricle sections from wild-type and *Nox4*$^{CM-/-}$ mice 7 days after treatment with vehicle or ISO. Data are Sirius red + area as a percent of total area (mean ± SEM, n = 6). Scale is 100 µm. **(B)** Flow cytometry analysis of LV single cell suspension for apoptotic cells from wild-type and *Nox4*$^{CM-/-}$ mice 1 day after treatment with vehicle or ISO. Data are a fraction of $PI^{-}ANXA5^{+}$ cells as a percent of all LV cells (mean ± SEM, n = 5). **(C)** Heart dry weight from wild-type and *Nox4*$^{CM-/-}$ mice 7 days after treatment with vehicle or ISO adjusted to the body weight (mean ± SEM, n = 12). **(D)** Representative pulsed-wave and tissue Doppler mode images from wild-type and *Nox4*$^{CM-/-}$ mice 7 days after treatment with vehicle or ISO. **(E–J)** Echocardiographic evaluation of ejection fraction (EF) **(E)**, LV end-diastolic volume (EDV) **(F)**, early diastolic filling wave peak velocity E **(G)**, early diastolic lengthening velocity E′ **(H)**, E/E′ ratio **(I)**, and deceleration time (DT) **(J)** was performed in wild-type and *Nox4*$^{CM-/-}$ mice 7 days after treatment with vehicle or ISO. Data are mean ± SEM, n = 8. **(K–N)** Left ventricle pressure-volume relationship analysis of ejection fraction (EF) **(K)**, end-diastolic pressure (EDP) **(L)**, end-diastolic pressure-volume relationship (EDPVR) **(M)**, and rate of pressure decrease (dP/dT_{min}) **(N)**. Data are mean ± SEM, n = 6.

that control mice had a 1.8-fold higher proportion of $CD11b^{+}$ cells than mice treated with GKT (Fig. 6G). On day 7 after ISO treatment, LV sections of control mice stained with picrosirius red had 1.9-fold higher collagen^{+} interstitial fibrosis area compared with hearts from GKT-treated mice (Fig. 6H). Mice treated with GKT had no changes in ejection fraction or end-diastolic volume 7 days after ISO treatment (Fig. 6I and J). In contrast, mitral valve peak E-velocity was decreased while septal E′-velocity was increased, followed by reduced E/E′ ratio, and longer mitral valve E-wave deceleration time after GKT treatment (Fig. 6K-N). These results demonstrate that NOX4 inhibition and mitochondrial ROS reduction in ISO-treated mice reduced inflammasome activation, cardiac inflammation, and fibrosis, thus preserving diastolic function.

4. Discussion

In the current study, we tested the hypothesis that CM NOX4-dependent mitochondrial ROS are critical mediators of inflammation

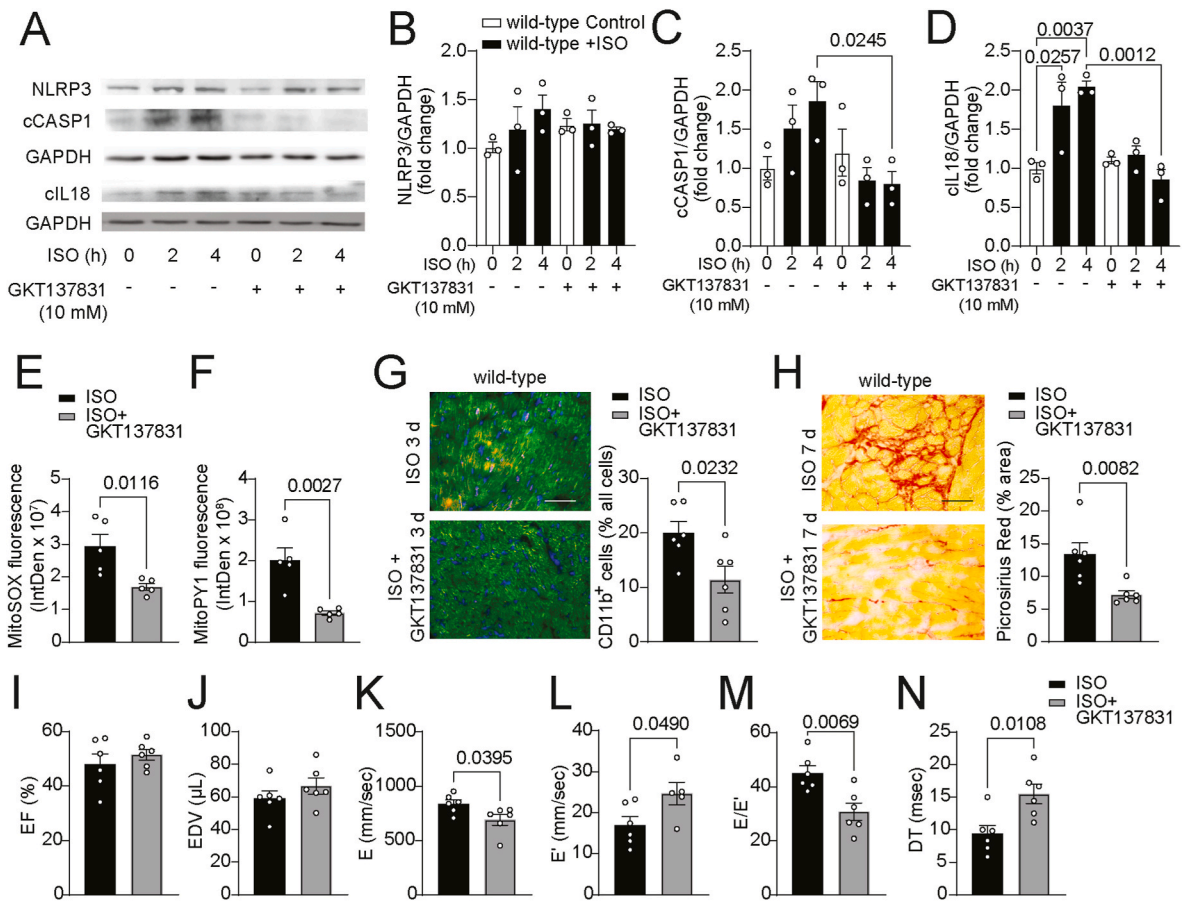

Fig. 6. NOX4 inhibition attenuates cardiac inflammation and fibrosis and preserves diastolic function in ISO-treated mice.
(A–D) Western blot analysis **(A)** and densitometric quantification of NLRP3 **(B),** cleaved caspase 1 **(C)** and cleaved IL18 **(D)** expression levels in mouse CM treated with ISO and with vehicle or GKT137831 for indicated times. Data are protein expression fold change relative to untreated control and adjusted for GAPDH levels (mean ± SEM, n = 3). **(E–F)** MitoSOX **(E)** and MitoPY1 **(F)** fluorescence were determined in microscopy images of the stained transverse left ventricle sections from wild-type mice 7 days after treatment with vehicle or ISO and GKT137831. Data are fluorescence integrated density (mean ± SEM, n = 5). **(G)** Representative fluorescence microscopy images and quantification of $CD11b^+$ cells in the transverse left ventricle sections from wild-type mice 3 days after treatment with ISO and GKT137831 stained for immunoreactive CD11b (red), MYH7(green), and DAPI (blue). Data are fractions of $CD11b^+$ cells as a percent of all cells in the FOV (mean ± SEM, n = 6). **(H)** Representative microscopy images and quantification of picrosirius red staining in the transverse left ventricle sections from wild-type mice 7 days after treatment with vehicle or ISO and GKT137831. Data are Sirius red + area as a percent of the FOV total area (mean ± SEM, n = 6). Scale is 100 µm. **(I–N)** Echocardiographic assessment of LV ejection fraction **(I)**, LV end-diastolic volume **(J)**, early diastolic filling E-wave velocity **(K)**, early diastolic lengthening velocity E' **(L)**, E/E′ ratio **(M)**, and deceleration time **(N)** was performed in wild-type mice 7 days after treatment with ISO and GKT137831. Data are mean ± SEM, n = 6.

and fibrosis in the development of stress cardiomyopathy. Our results demonstrate that: 1) upon β-adrenergic insult, CM mitochondrial ROS induced inflammasome activation, cytokine release, and the innate immune response with mobilization and expansion of cardiac embryonic-derived resident pro-inflammatory and pro-fibrotic macrophage population; 2) CM and activated macrophages induced fibroblasts activation with an increased proportion of collagen-secreting myo- and protomyo-fibroblasts; and 3) resultant excessive interstitial fibrosis leads to the development of restrictive diastolic dysfunction with increased LV stiffness and filling pressure. These data were supported by the observation that genetic deletion of CM *Nox4* or pharmacological inhibition NOX4 activity attenuated ISO-induced cardiac mitochondrial oxidative stress and inflammation, limiting the overall cardiac macrophage population while increasing the proportion of tissue-repair macrophages, reduced the proportion of collagen-secreting myofibroblasts, and preserved diastolic function.

As one of the major sources of intracellular H_2O_2 and a mediator of myocardial oxidative stress, NOX4 is implicated in the pathology of cardiomyopathy and diastolic dysfunction [20,39,40]. However, the actual mechanisms of late adverse outcomes in stress cardiomyopathy are less clear. Our results suggest that the interplay of cardiomyocyte NOX4-and mitochondria-dependent oxidative stress plays a critical role in the development of diastolic dysfunction secondary to sympathetic insult.

NOX4 expression and activity were significantly upregulated in the wild-type hearts shortly after ISO treatment. Similarly, *NOX4* was among the patients' most upregulated genes in LV biopsy samples during the acute but not in the functional recovery phases of Takotsubo cardiomyopathy [41]. This supports the role of NOX4 as a primary regulator of oxidative stress and inflammation during the early phase of cardiomyopathy. Congruent with that, mouse heart gene expression analysis after chronic ISO administration showed significant induction of *Nox4* expression along with genes involved in the acute phase and oxidative stress response [42].

A rapid inflammasome activation occurs in CM after stimulating heart β-adrenergic receptors without any initial priming [10]. Similar mechanisms have been proposed for NOX4 and mitochondrial-derived ROS activation of NLRP3 inflammasome [12,43]. In line with that, our current results demonstrate that ISO treatment stimulates CM inflammasome activity through β-adrenergic induction of NOX4-dependent mitochondrial ROS, whereas *Nox4* deletion or inhibition of NOX4 activity markedly reduced CM inflammasome activity and downstream

inflammatory responses without altering inflammasome expression. Our data are further supported by the evidence that mitochondrial ROS inhibition in mice attenuates the activation of CM inflammasome [44].

Myocardial inflammation and macrophage infiltration are induced by sympathetic stress [10]. Also, myocardial sympathetic overstimulation is associated with pro-inflammatory macrophage recruitment [22]. However, our detailed phenotyping of cardiac macrophages showed primarily embryonic-derived resident macrophage mobilization and proliferation with only minimal recruitment of non-classical Ly6C^{lo} monocytes after ISO treatment.

Cardiac resident macrophage populations are composed of heterogeneous self-renewing subsets with distinct functions [30,32]. Increased proportion of non-classical monocyte-derived patrolling tissue-repair macrophages (CCR2^{hi}Ly6C^{lo}CX3CR1^{hi}) [31] in wild-type but not *Nox4*$^{CM-/-}$ mouse hearts after ISO treatment may have been recruited by higher CCL2 levels in wild-type hearts. The loss of non-classical monocytes from circulation and their recruitment to the site of myocardial injury following coronary artery reperfusion was associated with decreased cardiac function and more adverse outcomes in STEMI patients [45]. Moreover, non-classical Ly6C^{lo} monocytes that express LGALS3 and TGFβ were implicated in fibrotic cardiac remodeling in patients with ischemic cardiomyopathy [46]. Congruent with this, an enriched subpopulation of non-classical Ly6C^{lo} cardiac macrophages that express higher levels of LGALS3 and TGFβ induces a pro-fibrotic environment and adverse cardiac remodeling in ISO-treated wild-type mice versus *Nox4*$^{CM-/-}$ mice.

A subset of embryonic-derived cardiac resident MHCII^{lo}CCR2^{-} macrophages display not inflammatory, but mostly reparative phenotypes and the ability to proliferate in response to cardiac injury [30]. Accordingly, our results revealed that wild-type mice were depleted of MHCII^{lo}CCR2^{-}CX3CR1^{lo} cardiac macrophages, while *Nox4*$^{CM-/-}$ mice had a larger percentage of these cells after ISO treatment. The findings support the notion that inhibiting NOX4-derived CM mitochondrial oxidative stress limits cardiac inflammation and monocyte recruitment, enhances the capacity of resident macrophages to limit adverse cardiac remodeling, and promotes recovery of heart function recovery following acute sympathetic stimulation.

In contrast to our observations, Liao et al. found a relative abundance of CCR2^{+} non-resident macrophages in the hearts of mice treated with high-dose ISO and depletion of resident macrophage populations [22]. These observations may be related to the use of a significantly higher ISO dose that was associated with local myocardial damage (increased troponin and apoptosis marker levels, impaired systolic function) as well as systemic inflammatory response (mobilization of pro-inflammatory Ly6C^{hi} monocytes) that defined early (1-day post-ISO) cardiac damage response. Similarly, RNA-seq analysis after 2 days of high-dose ISO injection showed an increase in monocyte-derived Ly6C^{+} resident macrophage cluster density but decreased CCR2^{-} resident macrophages in mice with stress-induced cardiomyopathy [47]. An acute high-dose catecholamine insult could conceivably result in a transient impairment of systolic function and increased monocyte-derived macrophage infiltration into the myocardium, whereas low-grade cardiac inflammation, fibrotic remodeling in the absence of CM apoptosis or necrosis, and diastolic dysfunction may be associated with the expansion of CCR2^{-} resident macrophage populations in low-dose catecholamine-induced cardiomyopathy.

Increased IL18 levels in the wild-type hearts after ISO treatment is consistent with previous reports [10,11]. Through direct paracrine effects, CM-derived IL18 activates cardiac macrophage inflammatory signaling, inducing LGALS3-mediated cardiac inflammation [11]. In addition, CM-derived IL18 may induce resident macrophage pro-inflammatory switch by inducing IFNγ secretion by activated resident macrophages and T-cells [48].

Increased mitochondrial stress and dysfunction in the heart can trigger the release of pro-fibrotic cytokines, the activation of cardiac fibroblasts, excessive ECM deposition, and passive stiffening of the myocardium [20]. Identification of an enriched cluster of resident macrophages with increased expression of IL6, TGFβ, and LGALS3 in wild-type mice after ISO treatment is consistent with that. Combined with increased cardiac IL18 levels, this led to the enrichment of activated collagen-secreting fibroblast populations and interstitial fibrosis in wild-type, but not in *Nox4*$^{CM-/-}$ mice. A stress-induced enrichment of ACTA2-negative collagen-secreting protomyofibroblast clusters coincided with the depletion of ACTA2-positive myofibroblast clusters. These findings indicate that fibrotic cardiac remodeling can occur without the differentiation of fibroblasts into myofibroblasts in HFpEF models associated with metabolic dysfunction [49]. In contrast, fibroblast markers measured 7 days after ISO treatment showed significantly higher levels of POSTN and ACTA2 in the wild-type mice, which is consistent with the fibrotic remodeling in diastolic dysfunction [20].

In our current study, mitochondrial oxidative stress in CM and myocardial interstitial fibrosis as well as diastolic dysfunction was reduced in ISO-injected mice treated with GKT137831, which agrees with previous observations of GKT137831 preserving diastolic function in a mouse model of mitochondrial oxidative stress [20].

The results of our study showing a reduction in CM mitochondrial oxidative stress and interstitial fibrosis and diastolic dysfunction in ISO-injected mice treated with GKT137831 are in line with our previous observations demonstrating preservation of diastolic function with GKT137831 treatment in a mouse model of mitochondrial oxidative stress. Interestingly, canagliflozin treatment in rats attenuated ISO-induced cardiac NOX4 expression, oxidative stress, and inflammation [50], indicating that it is feasible to target myocardial NOX4 activity. The results of our study are also consistent with previous reports that targeting IL18 with neutralizing antibodies [10] and downstream signaling including LGALS3 [11] may result in reduced cardiac inflammation and preservation of diastolic function in patients with stress cardiomyopathy.

Our study had some limitations. 1) Despite the fact that we cannot exclude the effects of ROS on CM relaxation, our functional studies did not support the presence of impaired cardiomyocyte relaxation induced by ISO at the experimental time points. A direct assessment of CM contraction/relaxation may provide additional evidence. 2) We used a limited number of cell-specific markers in the spectral flow cytometry to characterize multiple heart cell populations. It is possible that other immune cells may be involved in cardiac inflammation as well as in the activation of resident macrophages in response to the ISO challenge [22]. To determine whether neutrophils, dendritic cells, or T-cells are involved in cardiac inflammation and remodeling, additional immunophenotyping will be required. 3) All experiments were performed in male mice since it has been reported that incidence of stress cardiomyopathy is higher in post-menopausal women [1], whereas animal studies have shown that estrogen modulates adrenoreceptor signaling in the heart to reduce stress-induced cardiomyopathy [51].

Our results provide evidence that CM mitochondrial oxidative stress causes changes in myocardial structure and function in stress cardiomyopathy by inducing myocardial inflammation and by activation of embryonic-derived resident macrophages. In response to the increased expression of pro-fibrotic factors, protomyofibroblasts and myofibroblasts are activated, which results in interstitial collagen deposition, impairing diastolic function. Targeting myocardial mitochondrial ROS and/or resident macrophages may preserve cardiac function during acute sympathetic stress.

Declaration of competing interest

Marschall S. Runge is a member of the Board of Directors at Eli Lilly and Company. Other authors have declared that no conflict of interest exists.

Data availability

Data will be made available on request.

Acknowledgements

This work was supported by the Michigan Medicine-PKUHSC Joint Institute for Translational and Clinical Research Discovery Award (U063426) to NRM and YYZ.

Appendix A. Supplementary data

Supplementary data to this article can be found online at https://doi.org/10.1016/j.redox.2023.102937.

References

[1] C. Templin, J.R. Ghadri, J. Diekmann, L.C. Napp, D.R. Bataiosu, M. Jaguszewski, V. L. Cammann, A. Sarcon, V. Geyer, C.A. Neumann, B. Seifert, J. Hellermann, M. Schwyzer, K. Eisenhardt, J. Jenewein, J. Franke, H.A. Katus, C. Burgdorf, H. Schunkert, C. Moeller, H. Thiele, J. Bauersachs, C. Tschope, H.P. Schultheiss, C. A. Laney, L. Rajan, G. Michels, R. Pfister, C. Ukena, M. Bohm, R. Erbel, A. Cuneo, K. H. Kuck, C. Jacobshagen, G. Hasenfuss, M. Karakas, W. Koenig, W. Rottbauer, S. M. Said, R.C. Braun-Dullaeus, F. Cuculi, A. Banning, T.A. Fischer, T. Vasankari, K. E. Airaksinen, M. Fijalkowski, A. Rynkiewicz, M. Pawlak, G. Opolski, R. Dworakowski, P. MacCarthy, C. Kaiser, S. Osswald, L. Galiuto, F. Crea, W. Dichtl, W.M. Franz, K. Empen, S.B. Felix, C. Delmas, O. Lairez, P. Erne, J.J. Bax, I. Ford, F. Ruschitzka, A. Prasad, T.F. Luscher, Clinical features and outcomes of Takotsubo (stress) cardiomyopathy, N. Engl. J. Med. 373 (2015) 929–938, https://doi.org/10.1056/NEJMoa1406761.

[2] B.A. Sealove, S. Tiyyagura, V. Fuster, Takotsubo cardiomyopathy, J. Gen. Intern. Med. 23 (2008) 1904–1908, https://doi.org/10.1007/s11606-008-0744-4.

[3] H. Medina de Chazal, M.G. Del Buono, L. Keyser-Marcus, L. Ma, F.G. Moeller, D. Berrocal, A. Abbate, Stress cardiomyopathy diagnosis and treatment: JACC state-of-the-art review, J. Am. Coll. Cardiol. 72 (2018) 1955–1971, https://doi.org/10.1016/j.jacc.2018.07.072.

[4] K. Medeiros, M.J. O'Connor, C.F. Baicu, T.P. Fitzgibbons, P. Shaw, D.A. Tighe, M. R. Zile, G.P. Aurigemma, Systolic and diastolic mechanics in stress cardiomyopathy, Circulation 129 (2014) 1659–1667, https://doi.org/10.1161/CIRCULATIONAHA.113.002781.

[5] C. Neil, T.H. Nguyen, A. Kucia, B. Crouch, A. Sverdlov, Y. Chirkov, G. Mahadavan, J. Selvanayagam, D. Dawson, J. Beltrame, C. Zeitz, S. Unger, T. Redpath, M. Frenneaux, J. Horowitz, Slowly resolving global myocardial inflammation/oedema in Tako-Tsubo cardiomyopathy: evidence from T2-weighted cardiac MRI, Heart 98 (2012) 1278–1284, https://doi.org/10.1136/heartjnl-2011-301481.

[6] L. Lachmet-Thebaud, B. Marchandot, K. Matsushita, C. Sato, C. Dagrenat, S. Greciano, F. De Poli, P. Leddet, M. Peillex, S. Hess, A. Carmona, C. Jimenez, J. Heger, A. Reydel, P. Ohlmann, L. Jesel, O. Morel, Impact of residual inflammation on myocardial recovery and cardiovascular outcome in Takotsubo patients, ESC Heart Fail 8 (2021) 259–269, https://doi.org/10.1002/ehf2.12945.

[7] C. Scally, A. Rudd, A. Mezincescu, H. Wilson, J. Srivanasan, G. Horgan, P. Broadhurst, D.E. Newby, A. Henning, D.K. Dawson, Persistent long-term structural, functional, and metabolic changes after stress-induced (Takotsubo) cardiomyopathy, Circulation 137 (2018) 1039–1048, https://doi.org/10.1161/CIRCULATIONAHA.117.031841.

[8] V.M. Ferreira, M. Marcelino, S.K. Piechnik, C. Marini, T.D. Karamitsos, N.A. B. Ntusi, J.M. Francis, M.D. Robson, J.R. Arnold, R. Mihai, J.D.J. Thomas, M. Herincs, Z.K. Hassan-Smith, A. Greiser, W. Arlt, M. Korbonits, N. Karavitaki, A. B. Grossman, J.A.H. Wass, S. Neubauer, Pheochromocytoma is characterized by catecholamine-mediated myocarditis, focal and diffuse myocardial fibrosis, and myocardial dysfunction, J. Am. Coll. Cardiol. 67 (2016) 2364–2374, https://doi.org/10.1016/j.jacc.2016.03.543.

[9] A.R. Lyon, R. Citro, B. Schneider, O. Morel, J.R. Ghadri, C. Templin, E. Omerovic, Pathophysiology of Takotsubo syndrome: JACC state-of-the-art review, J. Am. Coll. Cardiol. 77 (2021) 902–921, https://doi.org/10.1016/j.jacc.2020.10.060.

[10] H. Xiao, H. Li, J.J. Wang, J.S. Zhang, J. Shen, X.B. An, C.C. Zhang, J.M. Wu, Y. Song, X.Y. Wang, H.Y. Yu, X.N. Deng, Z.J. Li, M. Xu, Z.Z. Lu, J. Du, W. Gao, A. H. Zhang, Y. Feng, Y.Y. Zhang, IL-18 cleavage triggers cardiac inflammation and fibrosis upon beta-adrenergic insult, Eur. Heart J. 39 (2018) 60–69, https://doi.org/10.1093/eurheartj/ehx261.

[11] G. Hu, J. Wu, H. Gu, X. Deng, W. Xu, S. Feng, S. Wang, Y. Song, Z. Pang, X. Deng, A. E. Vendrov, N.R. Madamanchi, M.S. Runge, X. Wang, Y. Zhang, H. Xiao, E. Dong, Galectin-3-centered paracrine network mediates cardiac inflammation and fibrosis upon beta-adrenergic insult, Sci. China Life Sci. 66 (2023) 1067–1078, https://doi.org/10.1007/s11427-022-2189-x.

[12] R. Zhou, A.S. Yazdi, P. Menu, J. Tschopp, A role for mitochondria in NLRP3 inflammasome activation, Nature 469 (2011) 221–225, https://doi.org/10.1038/nature09663.

[13] S. Toldo, C. Marchetti, A.G. Mauro, J. Chojnacki, E. Mezzaroma, S. Carbone, S. Zhang, B. Van Tassell, F.N. Salloum, A. Abbate, Inhibition of the NLRP3 inflammasome limits the inflammatory injury following myocardial ischemia-reperfusion in the mouse, Int. J. Cardiol. 209 (2016) 215–220, https://doi.org/10.1016/j.ijcard.2016.02.043.

[14] E. Mezzaroma, S. Toldo, D. Farkas, I.M. Seropian, B.W. Van Tassell, F.N. Salloum, H.R. Kannan, A.C. Menna, N.F. Voelkel, A. Abbate, The inflammasome promotes adverse cardiac remodeling following acute myocardial infarction in the mouse, Proc. Natl. Acad. Sci. U.S.A. 108 (2011) 19725–19730, https://doi.org/10.1073/pnas.1108586108.

[15] J. Wu, E. Dong, Y. Zhang, H. Xiao, The role of the Inflammasome in heart failure, Front. Physiol. 12 (2021), 709703, https://doi.org/10.3389/fphys.2021.709703.

[16] J. Kuroda, T. Ago, S. Matsushima, P. Zhai, M.D. Schneider, J. Sadoshima, NADPH oxidase 4 (Nox4) is a major source of oxidative stress in the failing heart, Proc. Natl. Acad. Sci. U.S.A. 107 (2010) 15565–15570, https://doi.org/10.1073/pnas.1002178107.

[17] M.D. Stevenson, C. Canugovi, A.E. Vendrov, T. Hayami, D.E. Bowles, K.H. Krause, N.R. Madamanchi, M.S. Runge, NADPH oxidase 4 regulates inflammation in ischemic heart failure: role of soluble epoxide hydrolase, Antioxidants Redox Signal. 31 (2019) 39–58, https://doi.org/10.1089/ars.2018.7548.

[18] T. Theccanat, J.L. Philip, A.M. Razzaque, N. Ludmer, J. Li, X. Xu, S.A. Akhter, Regulation of cellular oxidative stress and apoptosis by G protein-coupled receptor kinase-2; the role of NADPH oxidase 4, Cell. Signal. 28 (2016) 190–203, https://doi.org/10.1016/j.cellsig.2015.11.013.

[19] T. Ago, J. Kuroda, J. Pain, C. Fu, H. Li, J. Sadoshima, Upregulation of Nox4 by hypertrophic stimuli promotes apoptosis and mitochondrial dysfunction in cardiac myocytes, Circ. Res. 106 (2010) 1253–1264, https://doi.org/10.1161/CIRCRESAHA.109.213116.

[20] A. Lozhkin, A.E. Vendrov, R. Ramos-Mondragon, C. Canugovi, M.D. Stevenson, T. J. Herron, S.L. Hummel, C.A. Figueroa, D.E. Bowles, L.L. Isom, M.S. Runge, N. R. Madamanchi, Mitochondrial oxidative stress contributes to diastolic dysfunction through impaired mitochondrial dynamics, Redox Biol. 57 (2022), 102474, https://doi.org/10.1016/j.redox.2022.102474.

[21] C. Scally, H. Abbas, T. Ahearn, J. Srinivasan, A. Mezincescu, A. Rudd, N. Spath, A. Yucel-Finn, R. Yuecel, K. Oldroyd, C. Dospinescu, G. Horgan, P. Broadhurst, A. Henning, D.E. Newby, S. Semple, H.M. Wilson, D.K. Dawson, Myocardial and systemic inflammation in acute stress-induced (Takotsubo) cardiomyopathy, Circulation 139 (2019) 1581–1592, https://doi.org/10.1161/CIRCULATIONAHA.118.037975.

[22] X. Liao, E. Chang, X. Tang, I. Watanabe, R. Zhang, H.W. Jeong, R.H. Adams, M. K. Jain, Cardiac macrophages regulate isoproterenol-induced Takotsubo-like cardiomyopathy, JCI Insight 7 (2022), https://doi.org/10.1172/jci.insight.156236.

[23] S.A. Dick, J.A. Macklin, S. Nejat, A. Momen, X. Clemente-Casares, M.G. Althagafi, J. Chen, C. Kantores, S. Hosseinzadeh, L. Aronoff, A. Wong, R. Zaman, I. Barbu, R. Besla, K.J. Lavine, B. Razani, F. Ginhoux, M. Husain, M.I. Cybulsky, C. S. Robbins, S. Epelman, Self-renewing resident cardiac macrophages limit adverse remodeling following myocardial infarction, Nat. Immunol. 20 (2019) 29–39, https://doi.org/10.1038/s41590-018-0272-2.

[24] A.E. Vendrov, N.R. Madamanchi, X.L. Niu, K.C. Molnar, M. Runge, C. Szyndralewiez, P. Page, M.S. Runge, NADPH oxidases regulate CD44 and hyaluronic acid expression in thrombin-treated vascular smooth muscle cells and in atherosclerosis, J. Biol. Chem. 285 (2010) 26545–26557, https://doi.org/10.1074/jbc.M110.143917.

[25] Y. Bao, B.C. Willis, C.R. Frasier, L.F. Lopez-Santiago, X. Lin, R. Ramos-Mondragon, D.S. Auerbach, C. Chen, Z. Wang, J. Anumonwo, H.H. Valdivia, M. Delmar, J. Jalife, L.L. Isom, Scn2b deletion in mice results in ventricular and atrial arrhythmias, Circ. Arrhythm. Electrophysiol. 9 (2016), https://doi.org/10.1161/CIRCEP.116.003923.

[26] A.E. Vendrov, K.C. Vendrov, A. Smith, J. Yuan, A. Sumida, J. Robidoux, M. S. Runge, N.R. Madamanchi, NOX4 NADPH oxidase-dependent mitochondrial oxidative stress in aging-associated cardiovascular disease, Antioxidants Redox Signal. 23 (2015) 1389–1409, https://doi.org/10.1089/ars.2014.6221.

[27] A.E. Vendrov, A. Sumida, C. Canugovi, A. Lozhkin, T. Hayami, N.R. Madamanchi, M.S. Runge, NOXA1-dependent NADPH oxidase regulates redox signaling and phenotype of vascular smooth muscle cell during atherogenesis, Redox Biol. 21 (2018), 101063, https://doi.org/10.1016/j.redox.2018.11.021.

[28] A.E. Vendrov, M.D. Stevenson, S. Alahari, H. Pan, S.A. Wickline, N.R. Madamanchi, M.S. Runge, Attenuated superoxide dismutase 2 activity induces atherosclerotic plaque instability during aging in hyperlipidemic mice, J. Am. Heart Assoc. 6 (2017), https://doi.org/10.1161/JAHA.117.006775.

[29] I. Takac, K. Schroder, L. Zhang, B. Lardy, N. Anilkumar, J.D. Lambeth, A.M. Shah, F. Morel, R.P. Brandes, The E-loop is involved in hydrogen peroxide formation by the NADPH oxidase Nox4, J. Biol. Chem. 286 (2011) 13304–13313, https://doi.org/10.1074/jbc.M110.192138.

[30] K.J. Lavine, S. Epelman, K. Uchida, K.J. Weber, C.G. Nichols, J.D. Schilling, D. M. Ornitz, G.J. Randolph, D.L. Mann, Distinct macrophage lineages contribute to disparate patterns of cardiac recovery and remodeling in the neonatal and adult heart, Proc. Natl. Acad. Sci. U.S.A. 111 (2014) 16029–16034, https://doi.org/10.1073/pnas.1406508111.

[31] M. Nahrendorf, F.K. Swirski, E. Aikawa, L. Stangenberg, T. Wurdinger, J. L. Figueiredo, P. Libby, R. Weissleder, M.J. Pittet, The healing myocardium sequentially mobilizes two monocyte subsets with divergent and complementary functions, J. Exp. Med. 204 (2007) 3037–3047, https://doi.org/10.1084/jem.20070885.

[32] S. Epelman, K.J. Lavine, A.E. Beaudin, D.K. Sojka, J.A. Carrero, B. Calderon, T. Brija, E.L. Gautier, S. Ivanov, A.T. Satpathy, J.D. Schilling, R. Schwendener, I. Sergin, B. Razani, E.C. Forsberg, W.M. Yokoyama, E.R. Unanue, M. Colonna, G. J. Randolph, D.L. Mann, Embryonic and adult-derived resident cardiac

macrophages are maintained through distinct mechanisms at steady state and during inflammation, Immunity 40 (2014) 91–104, https://doi.org/10.1016/j.immuni.2013.11.019.
[33] N.G. Frangogiannis, Cardiac fibrosis, Cardiovasc. Res. 117 (2021) 1450–1488, https://doi.org/10.1093/cvr/cvaa324.
[34] B. Hinz, S.H. Phan, V.J. Thannickal, A. Galli, M.L. Bochaton-Piallat, G. Gabbiani, The myofibroblast: one function, multiple origins, Am. J. Pathol. 170 (2007) 1807–1816, https://doi.org/10.2353/ajpath.2007.070112.
[35] T. Oka, J. Xu, R.A. Kaiser, J. Melendez, M. Hambleton, M.A. Sargent, A. Lorts, E. W. Brunskill, G.W. Dorn 2nd, S.J. Conway, B.J. Aronow, J. Robbins, J. D. Molkentin, Genetic manipulation of periostin expression reveals a role in cardiac hypertrophy and ventricular remodeling, Circ. Res. 101 (2007) 313–321, https://doi.org/10.1161/CIRCRESAHA.107.149047.
[36] I. Cucoranu, R. Clempus, A. Dikalova, P.J. Phelan, S. Ariyan, S. Dikalov, D. Sorescu, NAD(P)H oxidase 4 mediates transforming growth factor-beta1-induced differentiation of cardiac fibroblasts into myofibroblasts, Circ. Res. 97 (2005) 900–907, https://doi.org/10.1161/01.RES.0000187457.24338.3D.
[37] H. Khalil, O. Kanisicak, R.J. Vagnozzi, A.K. Johansen, B.D. Maliken, V. Prasad, J. G. Boyer, M.J. Brody, T. Schips, K.K. Kilian, R.N. Correll, K. Kawasaki, K. Nagata, J. D. Molkentin, Cell-specific ablation of Hsp47 defines the collagen-producing cells in the injured heart, JCI Insight 4 (2019), e128722, https://doi.org/10.1172/jci.insight.128722.
[38] M.T. Waddingham, T. Sonobe, H. Tsuchimochi, A.J. Edgley, V. Sukumaran, Y. C. Chen, S.S. Hansra, D.O. Schwenke, K. Umetani, K. Aoyama, N. Yagi, D.J. Kelly, S. Gaderi, M. Herwig, D. Kolijn, A. Mugge, W.J. Paulus, T. Ogo, M. Shirai, N. Hamdani, J.T. Pearson, Diastolic dysfunction is initiated by cardiomyocyte impairment ahead of endothelial dysfunction due to increased oxidative stress and inflammation in an experimental prediabetes model, J. Mol. Cell. Cardiol. 137 (2019) 119–131, https://doi.org/10.1016/j.yjmcc.2019.10.005.
[39] D.F. Dai, T. Chen, H. Szeto, M. Nieves-Cintron, V. Kutyavin, L.F. Santana, P. S. Rabinovitch, Mitochondrial targeted antioxidant Peptide ameliorates hypertensive cardiomyopathy, J. Am. Coll. Cardiol. 58 (2011) 73–82, https://doi.org/10.1016/j.jacc.2010.12.044.
[40] M. Liu, E.M. Jeong, H. Liu, A. Xie, E.Y. So, G. Shi, G.E. Jeong, A. Zhou, S. C. Dudley Jr., Magnesium supplementation improves diabetic mitochondrial and cardiac diastolic function, JCI Insight 4 (2019), https://doi.org/10.1172/jci.insight.123182.
[41] H.M. Nef, H. Mollmann, C. Troidl, S. Kostin, T. Bottger, S. Voss, P. Hilpert, N. Krause, M. Weber, A. Rolf, T. Dill, J. Schaper, C.W. Hamm, A. Elsasser, Expression profiling of cardiac genes in Tako-Tsubo cardiomyopathy: insight into a new cardiac entity, J. Mol. Cell. Cardiol. 44 (2008) 395–404, https://doi.org/10.1016/j.yjmcc.2007.10.015.
[42] C.L. Galindo, M.A. Skinner, M. Errami, L.D. Olson, D.A. Watson, J. Li, J. F. McCormick, L.J. McIver, N.M. Kumar, T.Q. Pham, H.R. Garner, Transcriptional profile of isoproterenol-induced cardiomyopathy and comparison to exercise-induced cardiac hypertrophy and human cardiac failure, BMC Physiol. 9 (2009) 23, https://doi.org/10.1186/1472-6793-9-23.
[43] J.S. Moon, K. Nakahira, K.P. Chung, G.M. DeNicola, M.J. Koo, M.A. Pabon, K. T. Rooney, J.H. Yoon, S.W. Ryter, H. Stout-Delgado, A.M. Choi, NOX4-dependent fatty acid oxidation promotes NLRP3 inflammasome activation in macrophages, Nat. Med. 22 (2016) 1002–1012, https://doi.org/10.1038/nm.4153.
[44] T. Suetomi, A. Willeford, C.S. Brand, Y. Cho, R.S. Ross, S. Miyamoto, J.H. Brown, Inflammation and NLRP3 inflammasome activation initiated in response to pressure overload by Ca(2+)/calmodulin-dependent protein kinase II delta signaling in cardiomyocytes are essential for adverse cardiac remodeling, Circulation 138 (2018) 2530–2544, https://doi.org/10.1161/CIRCULATIONAHA.118.034621.
[45] S.A. Marsh, C. Park, R.E. Redgrave, E. Singh, L. Draganova, S.E. Boag, L. Spray, S. Ali, I. Spyridopoulos, H.M. Arthur, Rapid fall in circulating non-classical monocytes in ST elevation myocardial infarction patients correlates with cardiac injury, FASEB J 35 (2021), e21604, https://doi.org/10.1096/fj.202100240R.
[46] S. Chumakova, O. Urazova, V. Shipulin, M. Vins, A. Pryakhin, I. Sukhodolo, A. Stelmashenko, L. Litvinova, Y. Kolobovnikova, E. Churina, V. Novitskiy, Galectin 3 and non-classical monocytes of blood as myocardial remodeling factors at ischemic cardiomyopathy, Int. J. Cardiol. Heart Vasc. 33 (2021), 100766, https://doi.org/10.1016/j.ijcha.2021.100766.
[47] T. Hayashi, S.K. Tiwary, K.J. Lavine, S. Acharya, M. Brent, L. Adamo, A. Kovacs, D. L. Mann, The programmed death-1 signaling axis modulates inflammation and LV structure/function in a stress-induced cardiomyopathy model, J. Am. Coll. Cardiol. Basic Trans. Science. 7 (2022) 1120–1139, https://doi.org/10.1016/j.jacbts.2022.05.006.
[48] H. Schindler, M.B. Lutz, M. Rollinghoff, C. Bogdan, The production of IFN-gamma by IL-12/IL-18-activated macrophages requires STAT4 signaling and is inhibited by IL-4, J. Immunol. 166 (2001) 3075–3082, https://doi.org/10.4049/jimmunol.166.5.3075.
[49] L. Alex, I. Russo, V. Holoborodko, N.G. Frangogiannis, Characterization of a mouse model of obesity-related fibrotic cardiomyopathy that recapitulates features of human heart failure with preserved ejection fraction, Am. J. Physiol. Heart Circ. Physiol. 315 (2018) H934–H949, https://doi.org/10.1152/ajpheart.00238.2018.
[50] R. Hasan, S. Lasker, A. Hasan, F. Zerin, M. Zamila, F.I. Chowdhury, S.I. Nayan, M. M. Rahman, F. Khan, N. Subhan, M.A. Alam, Canagliflozin attenuates isoprenaline-induced cardiac oxidative stress by stimulating multiple antioxidant and anti-inflammatory signaling pathways, Sci. Rep. 10 (2020), 14459, https://doi.org/10.1038/s41598-020-71449-1.
[51] X. Cao, C. Zhou, J. Chong, L. Fu, L. Zhang, D. Sun, H. Hou, Y. Zhang, D. Li, H. Sun, Estrogen resisted stress-induced cardiomyopathy through increasing the activity of beta(2)AR-Galphas signal pathway in female rats, Int. J. Cardiol. 187 (2015) 377–386, https://doi.org/10.1016/j.ijcard.2015.02.113.